https://doi.org/10.5194/egusphere-2022-718
Preprint. Discussion started: 11 August 2022

A modern-day Mars climate in the Met Office Unified Model: dry simulations

Danny McCulloch[1], Denis Sergeev[1], Nathan Mayne[1], Matthew Bate[1], James Manners[2], Ian Boutle[2,1], Benjamin Drummond[2], and Kristzian Kohary[1]

[1]Department of Physics and Astronomy, University of Exeter, Exeter, EX4 4QL, UK
[2]Met Office, FitzRoy Road, Exeter, EX1 3PB, UK

Correspondence: Danny McCulloch (dm575@exeter.ac.uk)

Abstract. We present results from the Met Office Unified Model (UM), a world-leading climate and weather model, adapted to simulate a dry Martian climate. We detail the adaptation of the basic parameterisations and analyse results from two simulations, one with radiatively active mineral dust, and one with radiatively inactive dust. These simulations demonstrate how the radiative effects of dust act to accelerate the winds and create a mid-altitude isothermal layer during the dusty season. We validate our model through comparison with an established Mars model, the Laboratoire de Météorologie Dynamique Mars Planetary Climate Model (PCM), finding good agreement in the seasonal wind and temperature profiles, but discrepancies in the predicted dust mass mixing ratio and conditions at the poles. This study validates the use of the UM for a Martian atmosphere, it highlights how the adaptation of an Earth GCM can be beneficial for existing Mars GCMs and provides insight into the next steps in our development of a new Mars climate model.

1 Introduction

Understanding Mars' climate has been the motivation for many missions and numerical models for decades and through these many of the mechanisms driving the Martian climate have been unveiled. With our expanding comprehension of Mars' climate, studies have been able to build, refine and apply 3-dimensional general circulation models (GCMs). Such models include, but are not limited to, the NASA AMES model (Pollack et al., 1993; Haberle et al., 2019) and the Laboratoire de Météorologie Dynamique Planetary Climate Model (PCM, see Forget et al., 1999; Millour et al., 2018). Through the use of numerical models we are able to characterise Mars with limited observational data, allowing us to simulate areas where observational data is limited (Read et al., 2015; Martínez et al., 2017). Through these efforts our understanding of many atmospheric processes has been refined, including the annual CO_2 cycle (Forget et al., 1998; Malin et al., 2001; Aharonson et al., 2004; Hayne et al., 2012; Holmes et al., 2018; Banfield et al., 2020), CO_2 availability in the interest of terraforming (Jakosky and Edwards, 2018), its hydrological cycle (Houben et al., 1997; Haberle et al., 2001; Brown et al., 2014; Shaposhnikov et al., 2016, 2018; Singh et al., 2018; Pál et al., 2019), its surface topography (Smith et al., 1999; Richardson and Wilson, 2002; Zalucha et al., 2010) and the effects of the climatically dominant dust cycle (Kahre and Haberle, 2010; Wang and Richardson, 2015; Forget and Montabone, 2017; Wang et al., 2018; Gebhardt et al., 2020; Ball et al., 2021; Chaffin et al., 2021). Simulations have been performed ranging

https://doi.org/10.5194/egusphere-2022-718
Preprint. Discussion started: 11 August 2022

in scale from global (Navarro et al., 2014; Streeter et al., 2020; Kass et al., 2020) to mesoscale levels (Montabone et al., 2006; Spiga and Forget, 2009; Newman et al., 2021).

There are, however, still processes which are difficult to capture in climate models. One of these is dynamically modelling annular shifts in CO_2 freezing and thawing and the subsequent change in surface pressure this causes (Paige and Wood, 1992; Forget et al., 1999; Haberle et al., 2008; Kahre and Haberle, 2010). Simulating this in a self-consistent way using a GCM is difficult and efforts so far have relied on parameterisations (described by Forget et al., 1998, 1999; Spiga et al., 2017; Singh et al., 2018; Gary-Bicas et al., 2020). Recent model developments by Way et al. (2017) have included the CO_2 effects dynamically, providing a promising avenue for development of existing Martian GCMs. This is beneficial because it captures secondary effects of CO_2 precipitation between the atmosphere and surface as it descends. Another major challenge these GCMs face is accurately underpinning the cause of inter-annual dust storms and characterising dust uplifting rates prior to and following the dust season (Mulholland et al., 2013; Spiga et al., 2013; Forget and Montabone, 2017). Parameterising the methods for dust uplifting has been essential to simulating the climate and weather of Mars, but has still required periodic manual adjustments in order to match observations (Montabone et al., 2020). This limits the efficacy and self-sufficiency of Martian climate models, leading to difficulty in simulating global dust storms that should occur without forcing across multiple years and difficulty in predicting more local dust storms. As Way et al. (2017) has highlighted by dynamically solving for pressure variation as a consequence of CO_2 precipitation, a more complete physical model capable of capturing dust processes should also have beneficial feedback on the system.

To work towards rectifying these gaps in our modelling capabilities, we have adapted the Unified Model (hereafter; UM) to the study of the Martian climate, as a foundation step in building a comprehensive Martian climate model complementary to existing modelling efforts. The UM is used routinely for Earth weather and climate modelling. It has also been used for other planetary climates, including Earth-like exoplanets (Boutle et al., 2017; Sergeev et al., 2020; Eager et al., 2020), hot Jupiters (Mayne et al., 2014; Lines et al., 2018; Drummond et al., 2018), and mini-Neptunes (Mayne et al., 2019). By adapting the existing and well tested Earth parameterizations to Martian conditions, we can model climate processes in comparative ways to existing Mars GCMs (e.g. the quantity of available dust and size of the particles in the atmosphere). Such steps are key if GCMs are to progress to characterising Mars' climate with less manual prescription of parameters (Forget and Montabone, 2017; Montabone et al., 2020). In this aspect, the UM is self-consistent, dynamically solving for dust availability and using that prognostically to simulate Martian dust content throughout the varying seasons. In this first study we focus on a dry climate, including orography and dust, and highlight the importance of capturing dust accurately and its influences on the Martian climate. We also show that our adapted UM simulations capture key large-scale features of the Martian atmospheric circulation, including a periodic dust cycle without prescription of fixed dust parameters.

In this paper, we present a description of the UM and the adaptations made for Martian climate (Sect. 2). Namely, we describe the key model adaptations to simulate a dry Martian climate, such as planetary variables (atmospheric composition and orbital parameters, Sect. 2.1), radiative transfer (Sect. 2.2), orography (Sect. 2.3), dust (Sect. 2.4) and atmospheric surface pressure (Sect. 4.1). In Sect. 3 we describe how we configure the UM output for analysis, including configuration for two scenarios where one features radiatively active Martian dust (RA dust) and one with radiatively inactive dust (RI dust). In

https://doi.org/10.5194/egusphere-2022-718
Preprint. Discussion started: 11 August 2022

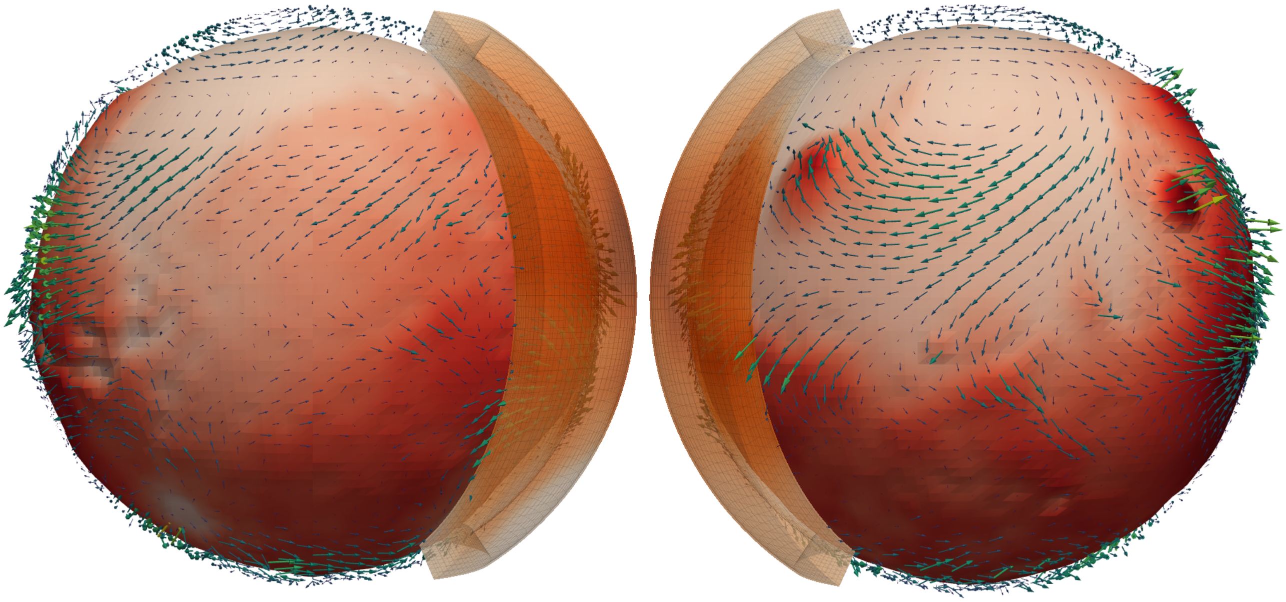

Figure 1. Overview 3D plot of example output during Southern Hemisphere summer (L_s=260°). Included is a segment of extracted regional dust layer as an isosurface, wind vectors at 1 km height (arrows) and orography (scaled up in this image by a factor of 30 to highlight extremities). Higher resolution GIF and code available at https://github.com/dannymcculloch/3d_Mars_gif.

Sect. 4 we present results from the two configurations of the UM for Mars and validate the UM with RA dust against the PCM. We highlight how differences in dust parameterization creates differences between outputs, both within the UM scenarios and between the RA UM and PCM, then discuss the reasons for these and their implications. Finally, in Sect. 5, we discuss how the model can be further developed to improve its accuracy, mainly via the inclusion of schemes capturing the effects of CO_2 ice and water vapour planned in future work.

2 Model description

For this study, we take the Global Atmosphere 7.0 science configuration of the UM (Walters et al., 2019) and adapt it to Martian conditions. The UM dynamical core (ENDGame, described by Wood et al., 2014) simulates the atmosphere as a non-hydrostatic fully compressible fluid and its numerical formulation uses a semi-implicit timestep and semi-Lagrangian advection scheme (Benacchio and Wood, 2016). A full description of the model's dynamical core is given by Staniforth and Wood (2003, 2008); Wood et al. (2014), with a global climate configuration further detailed by Walters et al. (2019). The benefit of using existing schemes in a GCM instead of creating new ones is that they capture essential atmospheric physics and are verified under a variety of conditions (e.g. dust on exoplanets Boutle et al., 2020). Fig. 1 shows an illustrative example of output from the UM configuration used to simulate the Martian climate.

https://doi.org/10.5194/egusphere-2022-718
Preprint. Discussion started: 11 August 2022

The UM grid configuration used in the present study has 90 by 144 grid points, corresponding to a resolution of 2° in latitude and 2.5° in longitude (i.e. a grid spacing of 118 and 147.5 km at the equator, respectively). This resolution allows us to accurately capture climate trends at a relatively high spatial resolution (Forget et al., 1999; Way et al., 2017), with even higher spatial resolutions available at a cost of increased computational power. This resolution is suitable for observing seasonal patterns within the Martian year (Navarro et al., 2014; Madeleine et al., 2011; Pottier et al., 2017), but higher spatial resolutions could readily be used to investigate selective regional climates (see for example, Sergeev et al., 2020)– a promising prospect for future applications.

In the vertical, we adopt 50 hybrid-height atmospheric levels up to a model top of 80 km above the areoid level. We use a quadratically stretched grid to enhance resolution near the surface. Levels nearer the surface follow the terrain, but are smoothed out gradually as the height increases, reaching a constant level height towards the highest altitudes (for our study this happens at ∼52 km, Wood et al., 2014). The level heights can be seen in table A2, where values are shown for a point with 0 m surface height.

For this study we use planetary parameters (Sect. 2.1), radiative transfer effects (Sect. 2.2), orography (Sect. 2.3), prognostic dust (Sect. 2.4) and pressure (Sect. 4.1) set to Martian values, with more description on each process in the respective section.

2.1 Planetary parameters

Mars has an eccentric orbit ($e = 0.0934$ compared to Earth's $e = 0.0167$) leading to an annual oscillation in the received irradiation. To capture this in the UM, we configure the model to run with this orbit starting from $0^\circ L_s$ (L_s is the ecliptic longitude of the sun), $0^\circ L_s$ corresponds to Northern Hemisphere (NH) spring equinox. We use stellar output for the present day Sun, but our simulated planet is placed at the Martian distance. Table 1 shows the values we implement for Mars' planetary values.

2.2 Radiative transfer

For calculating radiative transfer, we use the SOCRATES radiation scheme (described by Edwards and Slingo, 1996; Walters et al., 2019). This scheme uses a two-stream correlated-k method as described by Walters et al. (2019) and references therein. This scheme has been used extensively for studies of Earth (Spafford and Macdougall, 2021), in addition to hot Jupiters (Mayne et al., 2014), sub-Neptunes (Drummond et al., 2018) and rocky exoplanets (Boutle et al., 2020; Eager et al., 2020).

For radiative properties, we use an adapted version of the ROCKE-3D spectral files[1], which are appropriate for the CO_2-rich Martian atmosphere. We then added dust optical properties based on parameterisation from Walters et al. (2019). Mars' atmosphere primarily consists of CO_2 (∼95 %), N_2 (1.89 %) and Ar (∼1.93 %) (Read et al., 2015; Martínez et al., 2017); we simplify this to 95 % CO_2 and 5 % N_2 in our simulations. Ar was omitted in this study as the effects would be minimal on seasonal averages. The prescribed gas ratios throughout the atmosphere are assumed to be well mixed (Walters et al., 2019).

[1] Files sp_sw_42_dsa_mars_sun_3.8gya" and "sp_lw_17_dsa_mars_sun_3.8gya", available at https://portal.nccs.nasa.gov/GISS_modelE/ROCKE-3D/spectral_files/

https://doi.org/10.5194/egusphere-2022-718
Preprint. Discussion started: 11 August 2022

Table 1. Orbital, planetary and atmospheric parameters used to initialise the model

Orbital parameters used	
Epoch (Julian date)	2451545.0
Eccentricity	0.0934
Obliquity (radian)	∼0.4397
Mean acceleration due to gravity (m/s^2)	3.711
Solar irradiance at 1 AU (W/m^2)	1361.0
Semi-major axis (AU)	1.52368
Angular speed of planet rotation (radian/s)	$\sim 7.0882 \times 10^{-5}$
Radius (km)	3389.5
Gas constant for dry air	188.92
Mean scale height (m)	13.90×10^3

The Martian atmosphere features small amounts of water vapour which are generally increased during colder aphelion months (Nazari-Sharabian et al., 2020). This humidity affects the radiative transfer in every layer through water vapour molecules and cloud condensate (Shaposhnikov et al., 2016; Steele et al., 2017; Shaposhnikov et al., 2018; Fischer et al., 2019). Mars has water ice clouds which influence radiative transfer between the surface and the upper atmosphere (e.g. Navarro et al., 2014). For our setup, we use a completely dry atmosphere and surface. This is done to simplify the dust uplifting processes and to be able to correctly capture Martian seasonal trends initially. This allows for a benchmark comparison which can be expanded on in future studies, with a similar approach being carried out by Turbet et al. (2021).

In addition, we also use the terrain shading scheme described by Manners et al. (2012), which corrects the surface insolation depending on the zenith angle and obstructing elevation. This allows for a better representation of the effect that Martian orographical extremes have on their surroundings, e.g. the lone peak from Elysium Mons (25.02° N 147.21° E) casting a large shadow on the Northern Lowlands, or the depths of Valles Marineris canyons often being in a shade.

2.3 Orography

Orography affects various aspects of the Martian climate such as dust deposition and global circulation (Smith et al., 1999; Zalucha et al., 2010; Pottier et al., 2017). Dominant orographic features include the Tharsis region and Hellas Basin, but also a general hemispheric dichotomy featuring a higher southern hemisphere that gradually descends northward (Richardson and Wilson, 2002). Mars' hemispheric asymmetry heavily influences the atmospheric circulation, leading to large seasonal differences amplified by Mars' orbital eccentricity (Richardson and Wilson, 2002; Zalucha et al., 2010). Therefore, in order to better characterise Mars' climate and atmospheric processes, correctly capturing the surface elevation hemispheric dichotomy in Martian climate models is important (Zalucha et al., 2010).

https://doi.org/10.5194/egusphere-2022-718
Preprint. Discussion started: 11 August 2022

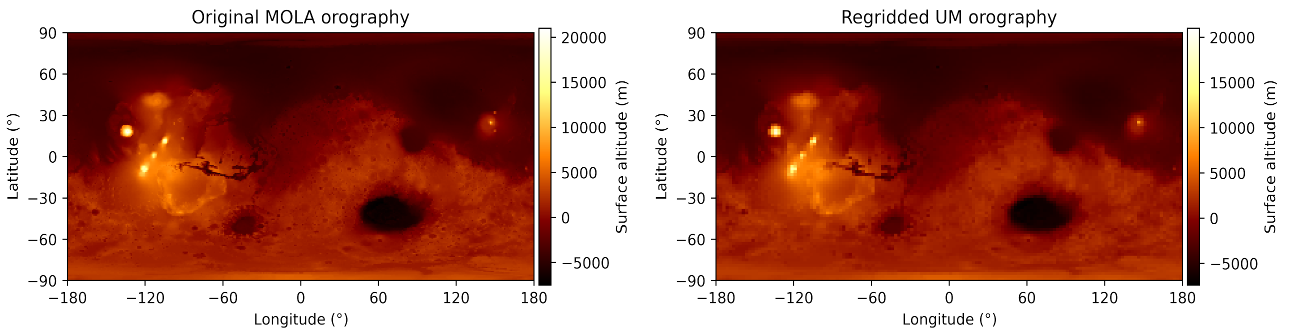

Figure 2. Original MOLA elevation data (left) compared to the regridded elevation data used in the UM (right). Colour scales are matching between plots.

For this study, we use the sub-grid orographic drag parameterisation already present and verified in the UM (as described in detail by Lott and Miller, 1997; Webster et al., 2003; Vosper, 2015; Walters et al., 2019) but for Martian values. We obtained the widely-used, high-resolution MOLA elevation data (Fig. 2a, described by Smith et al., 1999)[2]. We regrid the MOLA dataset to the resolution used in the current study. We choose to use the resolution of 90×144 as it allows for an adequate global representation needed to simulate global climate patterns present on Mars. In regridding, the cells from the original dataset that encompass a single grid cell are averaged which leads to some height loss at the highest peaks, where sub-grid elevation is varied. The effects of the regridding can be seen in Fig. 2b, where the MOLA dataset is compared to the regridded version. There is some inevitable height smoothing with regridding, Olympus Mons changes from 25km height to 19 km and the lowest parts of the Hellas Basin from -7.5km to -7.3km.

2.4 Dust and surface roughness

Dust is synonymous with Mars, it is a key driver in a wide range of atmospheric phenomena, ranging from mesoscale dust devils, effective at uplifting local surface dust (Neakrase et al., 2016), to global dust storms affecting global temperatures for long periods of time (Forget and Montabone, 2017; Wang et al., 2018; Streeter et al., 2020). Dust is a crucial contributor to the greenhouse effect on Mars. Because of this, large fluctuations in atmospheric dust content can have serious effects on the lower altitude temperatures (below $\sim$25 km) during global dust storms and has been well described by Streeter et al. (2020) and Wang and Richardson (2015). Dust also affects the diurnal cycle of temperatures, retaining thermal radiation during the night and reflecting solar radiation during the day (Madeleine et al., 2011). The dust quantities vary across the Martian year, with months 6 to 12 (month timings shown in Table A1) having much higher atmospheric dust than the other months (Forget and Montabone, 2017). Months 1 to 6 are generally colder on Mars, leading to weaker wind speeds and subsequently less dust

[2]MOLA dataset available at: https://astrogeology.usgs.gov/search/map/Mars/Topography/HRSC_MOLA_Blend/Mars_HRSC_MOLA_BlendDEM_Global_200mp_v2

https://doi.org/10.5194/egusphere-2022-718
Preprint. Discussion started: 11 August 2022

uplifting during the colder months. Intra-annual shifts from the dust storm season to a colder less dusty season is difficult to self-consistently capture in 3D GCMs (Madeleine et al., 2011; Forget and Montabone, 2017).

We adapt the dust scheme available in the UM, which handles dust parameterisation using 9 particle radial size bins (0.03–1000 μm). A normalised distribution characterising the surface dust is set, with the values in bins 1–6 (0.03–30 μm) prescribed and the remaining dust equally distributed across bins 7–9 (30–1000 μm). This is described in detail by Woodward (2001, 2011) and an example of its application in a non-Earth climate can be seen in Boutle et al. (2020). Atmospheric dust is absent upon initialisation and is calculated throughout the model simulation. Dust particles are transported by atmospheric dynamics, turbulence (Lock et al., 2000), saltation (for uplifting larger particles, Woodward, 2001; Woodward et al., 2022) and dry deposition. Absorption and scattering of short/long-wave radiation is calculated using Mie theory with the assumption that dust particles are spherical.

To determine the size distribution for the respective dust bins in the UM for Mars, we applied the same formula as used by Madeleine et al. (2011) namely

$$n(r) = \frac{N}{\sqrt{2\pi}\,\sigma_0\, r} \exp\left[-\frac{1}{2}\left(\frac{\ln(r/r_0)}{\sigma_0}\right)^2\right], \tag{1}$$

where r is the potential size of the dust particle, between 0.03 and 30 microns. σ_0 is the variance and r_0 is the mean, given by Madeleine et al. (2011). N is the normalised (to unity) maximum number of particles available and $n(r)$ is the probability of dust radii being present dependant on r. This provides the distribution presented in Fig. 3, giving the probable radial size of any given particle. The dust bin size ranges used have been overlaid with coloured bars for each bin. The majority of dust resides in bin 4, but all bins are used in this study.

Dust lifting depends on the aerodynamic roughness length via a parameterization incorporating a variety of factors (e.g. wind erosion, friction, drag, etc). This could be set to a constant value in order to make sure that dust is being uplifted equally across the planet, but this is likely to oversimplify the climate. In the UM, we use the aerodynamic roughness length map from Hébrard et al. (2012), shown in Fig. 4. By using these values, we are able to simulate regional dust uplifting dispersion, as opposed to a globally uniform dust uplifting rate (Hébrard et al., 2012).

3 Experimental setup

We initialise the UM from a motionless atmospheric state with a uniform surface temperature of 250 K and surface pressure of 610 Pa. Other variable schemes are also initialised at this stage (orography, Sect. 2.3, and dust, Sect. 2.4). The model is then integrated for 40 Martian years to achieve a steady state, which is determined as there being no inter-annual increase or decrease in the balance between incoming and outgoing radiation at the top of the atmosphere (TOA) between Martian years (with years averaged to omit for differences caused by orbit eccentricity). After this, the model is run for another Martian year, and this final year data is what is presented in this paper. The model output is provided every sol across a Martian year (668 sols/687 days). A sol is defined here as 24 hours and 40 minutes (simplified from a Martian solar day of 24 hours, 39 minutes

https://doi.org/10.5194/egusphere-2022-718
Preprint. Discussion started: 11 August 2022

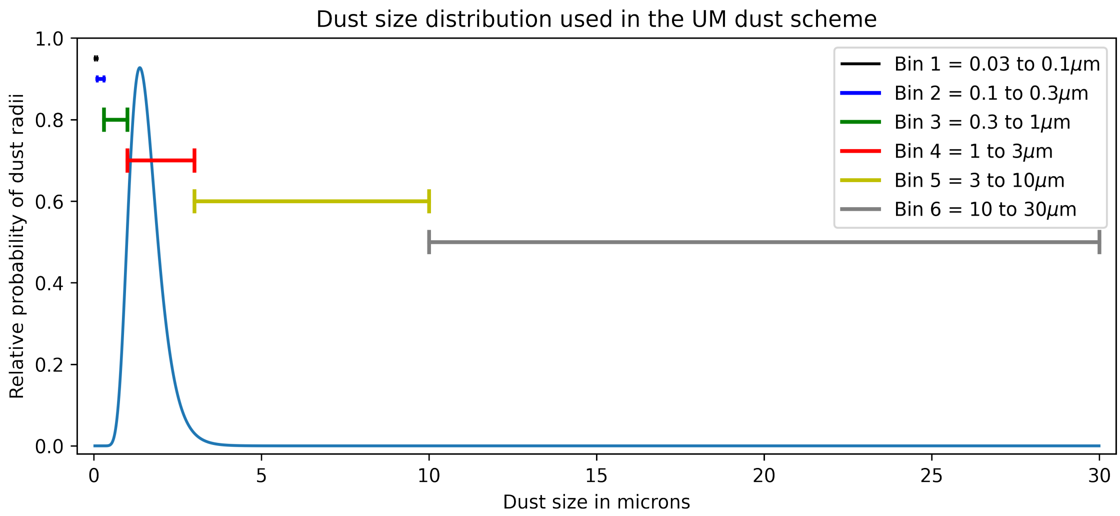

Figure 3. Dust size probability distribution used for the UM following Madeleine et al. (2011). Dust bin ranges are shown by the coloured bars.

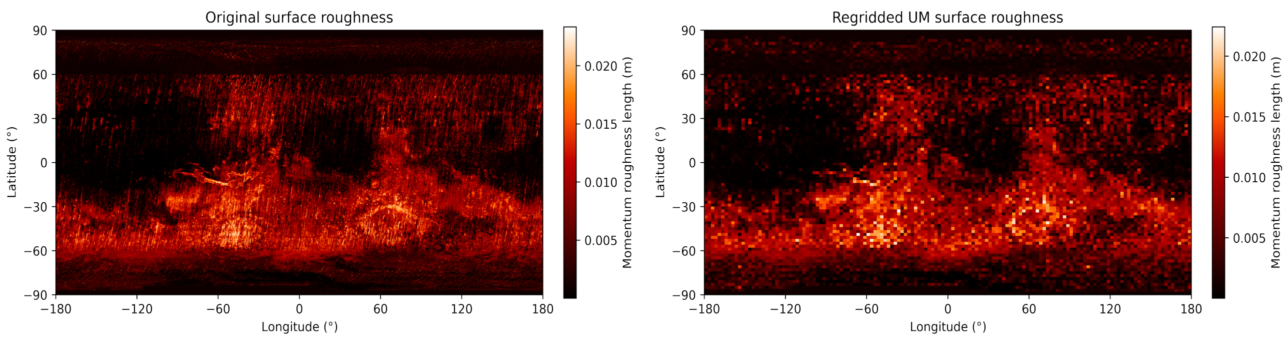

Figure 4. Surface roughness map from Hébrard et al. (2012) (left) and how it is represented in the UM after regridding (right).

and 35 seconds). For each model diagnostic, values are recorded every 5 minutes (20 minutes for radiation variables, e.g. TOA radiation flux) which is then averaged at the end of each sol. The year starts at 0° L_s then is run for 688 Earth days, taking an average across the sol. These sol outputs are then aggregated into Martian months (Table A1), this is done to better understand seasonal trends across the year and to match the data to time distributions present in other models (Forget et al., 1999).

To discern the effects of dust in the UM, we perform two separate simulations, one with radiatively active (RA) dust and one with radiatively inactive (RI) dust. Both setups are identical in every other way (e.g. spin-up time, orography, orbital parameters, etc). For RI dust, the dust sizes and quantities are still prescribed, but all radiative effects of dust are switched off. This allows us to observe the effects of a dust scheme in our Mars setup versus what would already occur without the presence of atmospheric dust. This is useful for a variety of reasons. It allows us to highlight spatial/temporal regions of interest where

https://doi.org/10.5194/egusphere-2022-718
Preprint. Discussion started: 11 August 2022

dust might originate from, particularly where there are differences between scenarios. It also allows us to begin to distinguish the exclusive influence of dust, as any differences between scenarios can be attributed to this one variable.

To ensure that the UM reproduces seasonal patterns with sufficient accuracy, we compare our results to those of an established Mars GCM. In this study, we use year average (an average of all years where a dust storm did not occur) results from the Mars Climate Database[3], which provides output from the PCM (Forget et al., 1999; Millour et al., 2018). This dataset has 49 points in latitude and 64 points in longitude, with 30 layers in the vertical extending up to 108 km. The output is also separated into the same Martian months as prescribed in the UM (e.g. Martian month 1 = sols 0 to 61, as per Table A1). It features dust (Madeleine et al., 2011), a hydrological cycle (Navarro et al., 2014), a CO_2 ice cycle (Forget et al., 1998, 1999), atmospheric ozone (Lefèvre et al., 2008) and an upper atmosphere layer above 80 km (Colaïtis et al., 2013; González-Galindo et al., 2015).

The PCM uses a terrain-following pressure-based vertical coordinate $\sigma = p/p_s$, where p_s & p are the surface pressure & atmospheric pressure respectively, which is different to the UMs height-based vertical coordinate (Forget et al., 1999; Wood et al., 2014). This presents a difficulty in precise comparison between model simulations, as results cannot be compared straightforwardly without some form of interpolation. Furthermore, the UM and PCM have different upper boundaries, which requires datasets to be cropped until height is matched. Therefore, to validate our model against the PCM, we linearly interpolate the UM output to σ levels at each output timestep, focusing on the levels where there is sufficient data for both models at the same pressure (σ ranging from 1 at the surface to 0.01 in the upper atmosphere). As we are concerned with the large–scale, seasonal, climate we compare zonal, monthly averages of the UM outputs to those of the PCM.

4 Results

In the following sections we show Mars' annual mean pressure observations at the *Viking* lander sites compared to the UM (Sect. 4.1). We then describe Mars' climate seasonality and how this is portrayed in simulations (Sect. 4.2). We then highlight the key differences between the RA dust scenario and PCM in more detail (Sect. 4.3). In particular, we focus on dust differences in our results and discuss further the implications of this (Sect. 4.3.3).

4.1 Atmospheric pressure

Mars undergoes annual fluctuations in surface pressure, decreasing during colder months and increasing during the dust season. This is mainly due to net freezing and thawing of polar ice caps, which extracts and releases atmospheric CO_2, respectively. The mean surface pressure on Mars is much lower than on Earth, resulting in large diurnal temperature fluctuations and limiting dust loading capacity (Read et al., 2015; Martínez et al., 2017) due to less heat retention from the atmosphere. To show how pressure fluctuates in the UM, we show surface pressure across the Martian year at the approximate *Viking* lander sites in the model compared to observational data from the landers. The values from the UM are not from the exact spatial location of the landers, due to their positions being within grid cells, but instead is the closest data point to where the landers would be in the UM. Fig. 5 shows that the UMs observed pressure near the *Viking* lander 1 & 2 (VL1 & VL2) sites remain steady during

[3] Available at http://www-mars.lmd.jussieu.fr/

https://doi.org/10.5194/egusphere-2022-718
Preprint. Discussion started: 11 August 2022

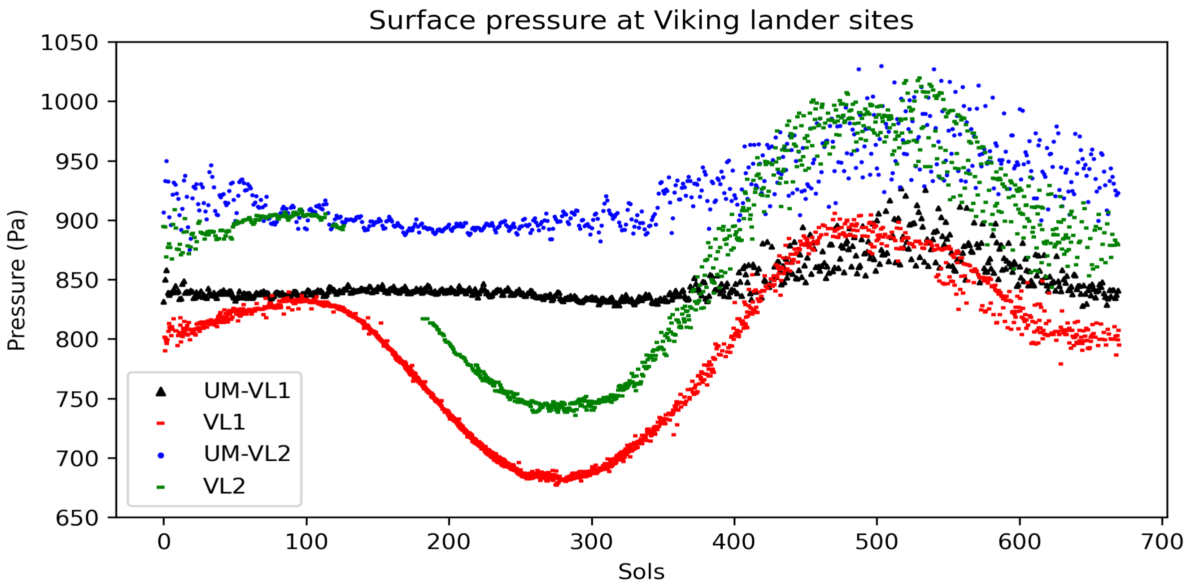

Figure 5. UM surface pressure at approximate *Viking* lander 1 & *Viking* lander 2 sites compared to observational data across a Martian year. *Viking* lander data available from Tillman (1989).

the colder months and increase during the dust season. As the UM does not currently have a CO_2 ice cycle, this cold season pressure drop present in observations is absent. This leads to a high disparity of pressures between sols 130–410 between simulated and observed pressures. The UM does capture a minor pressure increase during sols 410–530 despite the lack of a CO_2 ice scheme. This increase in pressure is likely due to a temperature increase as a result of higher solar radiation. The absence of a pressure decrease during months 2–6 would suggest that this could potentially be a secondary feedback effect caused by heating from atmospheric dust. Since atmospheric dust quantities are much lower in the colder months their effect is minimal, but as dust abundance increases, the magnitude of the effect of it is amplified increasing pressure further.

4.2 Overview of a year of Martian climate

To compare the results between RA dust, RI dust and the PCM we show outputs of four atmospheric variables for months 3, 6, 9 and 12 (sol breakdown given in Table A1). Output is zonally and temporally meaned across the sols of the given month. The variables are temperature (Fig. 8), zonal (eastward) winds (Fig. 6), meridional (northward) winds (Fig. 7) and dust mass mixing ratio (MMR, Fig. 9). The 3×4 format and month dates are consistent throughout the figures. We explain the development of Mars' climate across a typical year and how this is simulated in our results, we then compare these outputs across simulations.

https://doi.org/10.5194/egusphere-2022-718
Preprint. Discussion started: 11 August 2022

4.2.1 Month 3

During this period, Mars is close to its coldest. NH temperature maximums are ∼220K in the northerly latitudes for both scenarios, zonal and meridional winds are slower and uplifted dust quantities are low. Temperatures drop due to Mars' orbit taking the planet away from the Sun, which leads to a reduction in solar radiation and a net cooling for the atmosphere and surface. This leads to a variety of secondary effects occurring on Mars. CO_2 begins to freeze quicker than it thaws on the opposite pole leading to a global pressure reduction as CO_2 is sequestered from the atmosphere. Temperatures vary throughout the Martian year, but averages are lowest during aphelion months (Fig. 8, month 3) and highest during the dust season (Fig. 8, month 9). This temperature difference leads to weaker winds during month 3 and less dust uplifting, leading to less dust MMR throughout the majority of aphelion compared to months during perihelion (Read et al., 2015). Temperatures are highest in the NH where it is summer, then gradually decrease southward. Temperatures also decrease as height increases, as is to be expected. In terms of atmospheric circulation, Mars features strong zonal jets that alternate between hemispheres throughout the year, occurring during winter seasons to the respective hemisphere as the planet transitions between seasons (Fig. 6). Meridional winds feature a weak jet near the equator surface, with an opposing jet at the upper boundary layer at $\sim 0.4\ \sigma$ (Fig. 7). The UM RA dust and RI dust simulations are quite similar in month 3, with zonal wind differences of about ≈3 m s^{-1} and temperature differences of $\approx 3\,K$. This is likely due to the low levels of dust abundance and thus its radiative impact during this time period (Fig. 9, month 3).

The UM and the PCM both feature strong zonal jets in the upper atmosphere in the SH, but the UMs winds are slower at the upper boundary at the equator and in the NH zonal jet (Fig. 6). The UM features a stronger meridional jet near the surface, but the jet present in the PCM near the top of the atmosphere is much lower and slower in the UM (by ~ 4 m s^{-1}, Fig. 7). Air temperature in the UM is generally lower, with especially strong differences between model outputs at the poles, negative at the south pole and positive at the north pole. The lower atmospheric temperature is likely caused by less dust in the atmosphere. Its radiative effects are minimal in the UM, whilst it is relatively abundant in the PCM (average temperature difference omitting the poles of ≈-15 K, Fig. 8). The temperature differences at the poles (exceeding -30 and 30 K at either pole), which are much greater than those closer to the equator, are mainly due to the absence of polar ice in the UM, with the latent heat transfer and surface optical properties of ice being simulated in the PCM (Fig. 8). Lastly, dust differences between model outputs are at their highest, relative to concentration comparisons between models in each month. The UM simulates far less atmospheric dust than the PCM. This is likely due to the absence of forced dust uplifting in the UM which is present in the PCM (described by Madeleine et al., 2011; Spiga et al., 2013; Montabone et al., 2020).

4.2.2 Month 6

Here, Mars' hemispheres are transitioning seasons, this can be seen in the jet reversal in the zonal winds and by the location of the temperature maxima in the lower latitudes. Mars features a single Hadley cell which reverse twice a year, with polar cells at each pole. Dust MMR is more than month 3 due to rising temperatures increasing wind speeds and there are larger concentrations forming near the equator (Fig. 9). Despite this, dust in the RA scenario is uplifted more compared to RI by ∼10

https://doi.org/10.5194/egusphere-2022-718
Preprint. Discussion started: 11 August 2022

%. The reason for this difference is likely due to uplifted RA dust scattering solar radiation close to the surface, causing more near-surface warming than there would be with RI dust. Where the increased temperature causes faster near-surface winds increasing dust uplifting rates. Temperature differences between the RA and RI scenarios (Fig. 8) are between -5 and 5 K which is more than in month 3, but lower than later months. There is a clear difference between polar regions in opposing directions (colder NH pole and warmer SH pole), in addition to a mid-altitude band of warmer air by up to 3 K in the RA dust scenario. These indicate that dust is beginning to impact the atmosphere more actively. Zonal winds are also reflecting the increasing differences (Fig. 6), with a NH polar zonal jet difference of up to 40 m s^{-1}. Meridional winds differences are still minimal (Fig. 7), but there are some differences forming which are amplified in later months. Mars' seasonal cycle and the associated reversal of its Hadley cell during this month are clearly shown in the meridional wind patterns, with counter-flowing jets present in months 6 but more stable meridional winds during months 3, 9 and 12.

Differences between the UM RA dust scenario and PCM here are varied in their magnitude, but present for each variable. For air temperatures (Fig. 8), the UM is comparable at the surface near the equator, but temperature in the UM decreases quicker with height up to the upper atmosphere. The UM, however, features a region with higher temperatures at ∼60° S latitude, which reaches ∼24 K at the surface, but gradually decreases with height. There are still differences between the models at the poles, but these differences are less substantial than they were during month 3 (now down to a difference of the UM being -16 K compared to the PCM at the surface). Zonal winds feature a variety of differences between models, with faster and slower zonally averaged wind speeds distributed across the atmosphere. Both models feature polar jets in both hemispheres, but the UM zonal jets are slower than the PCMs by up to 40 m s^{-1} at the centre of the SH jet, which gradually becomes more comparable further from the centre of the jet towards the surface. There is an area of faster winds by ∼10 m s^{-1} in the UM at the SH pole, which is at the middle of the atmosphere and lessens towards the surface where differences again become 0. This is likely due to the SH polar jet in the UM being more stretched than the PCM, where the jet is spread over a larger area so winds are weaker. The polar jet in the NH is also slower in the UM by up to 30 m s^{-1}. Dust differences between models are still considerable throughout the entire atmosphere as in month 3, with the PCM having up to 1.2×10^{-5} kg kg^{1} (∼700 %) more dust than the UM near the surface, while differences lessen with height. Here, the UM dust quantities are much less than the PCM, but uplifting is increasing as Mars approaches the dust season. In all 3 scenarios dust concentration is increasing, this is promising as it shows the ability to dynamically simulate a substantial change in atmospheric dust abundance during a transition of seasons, as occurs on Mars.

https://doi.org/10.5194/egusphere-2022-718
Preprint. Discussion started: 11 August 2022

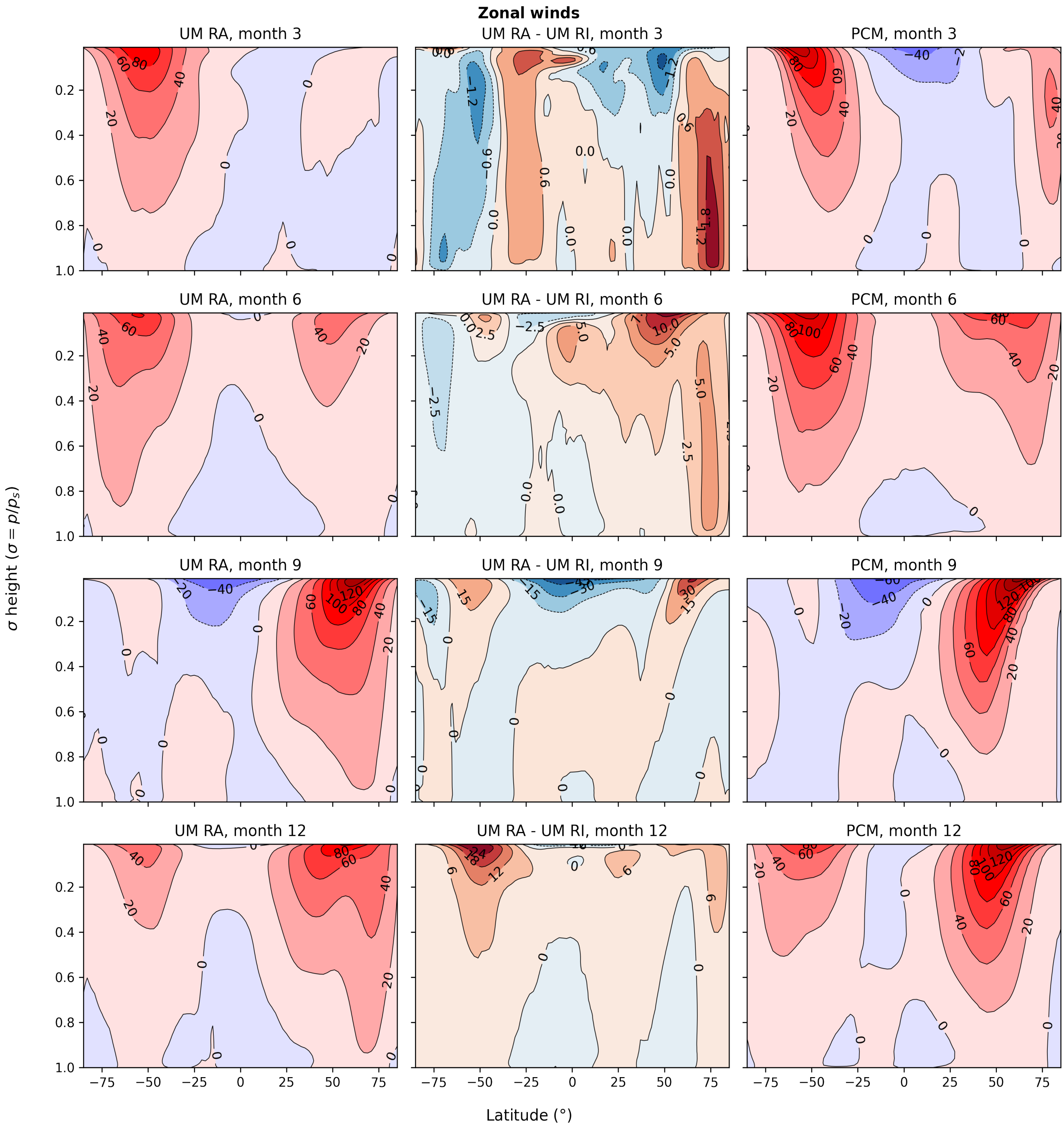

Figure 6. Zonal mean zonal winds (m s^{-1}) across 4 seasons within the Martian year. For each month, the time average is taken of all sols within that month. The RA dust scenario is shown on the left, differences between the RA and RI dust scenario in the centre and PCM output on the right. Colour scales on the left-hand and right-hand plots are matched across all months and between models.

https://doi.org/10.5194/egusphere-2022-718
Preprint. Discussion started: 11 August 2022

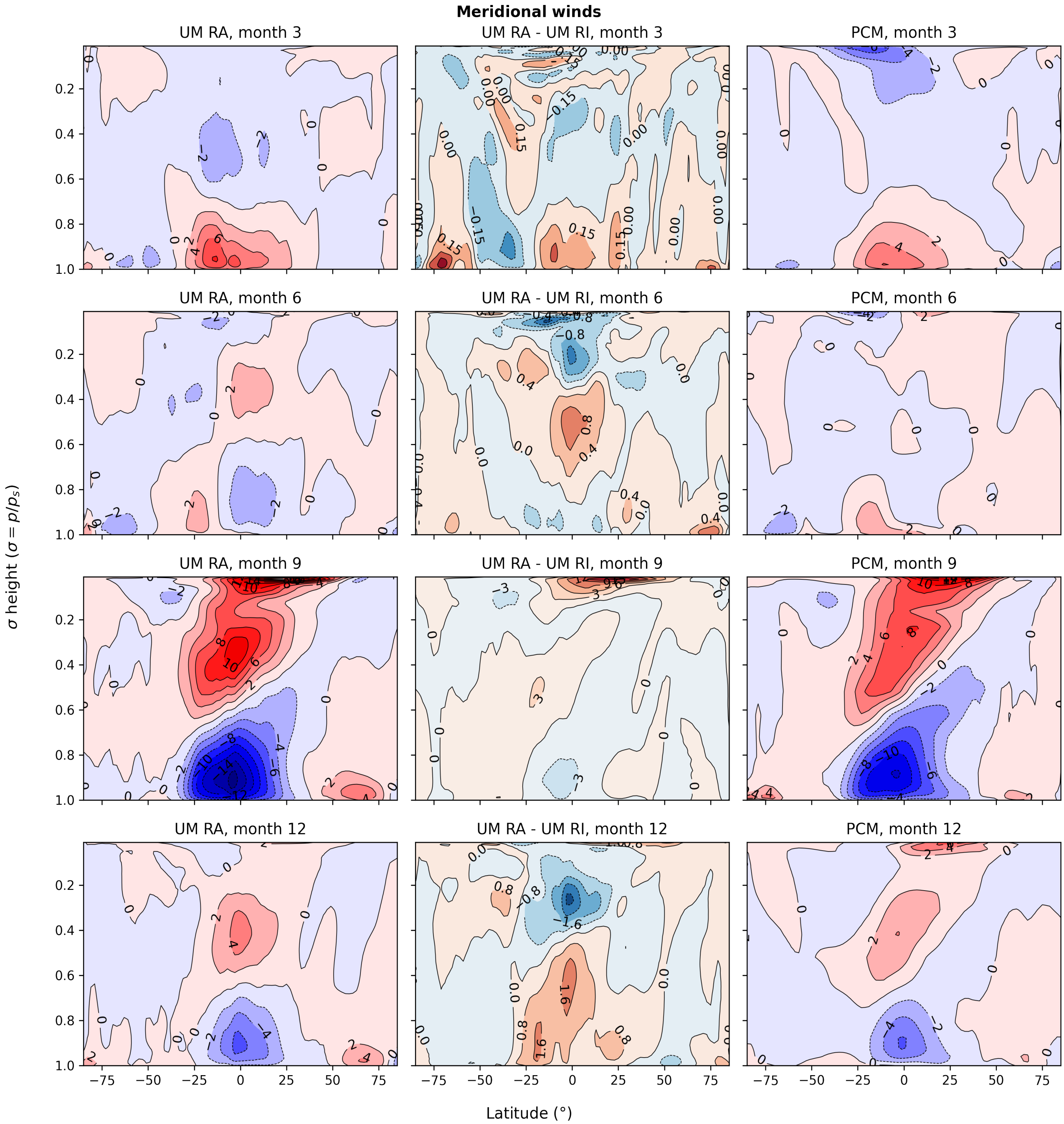

Figure 7. Zonal mean meridional winds (m s^{-1}) across 4 seasons within the Martian year. For each month, the time average is taken of all sols within that month. The RA dust scenario is shown on the left, differences between the RA and RI dust scenario in the centre and PCM output on the right. Colour scales on the left-hand and right-hand plots are matched across all months and between models.

https://doi.org/10.5194/egusphere-2022-718
Preprint. Discussion started: 11 August 2022

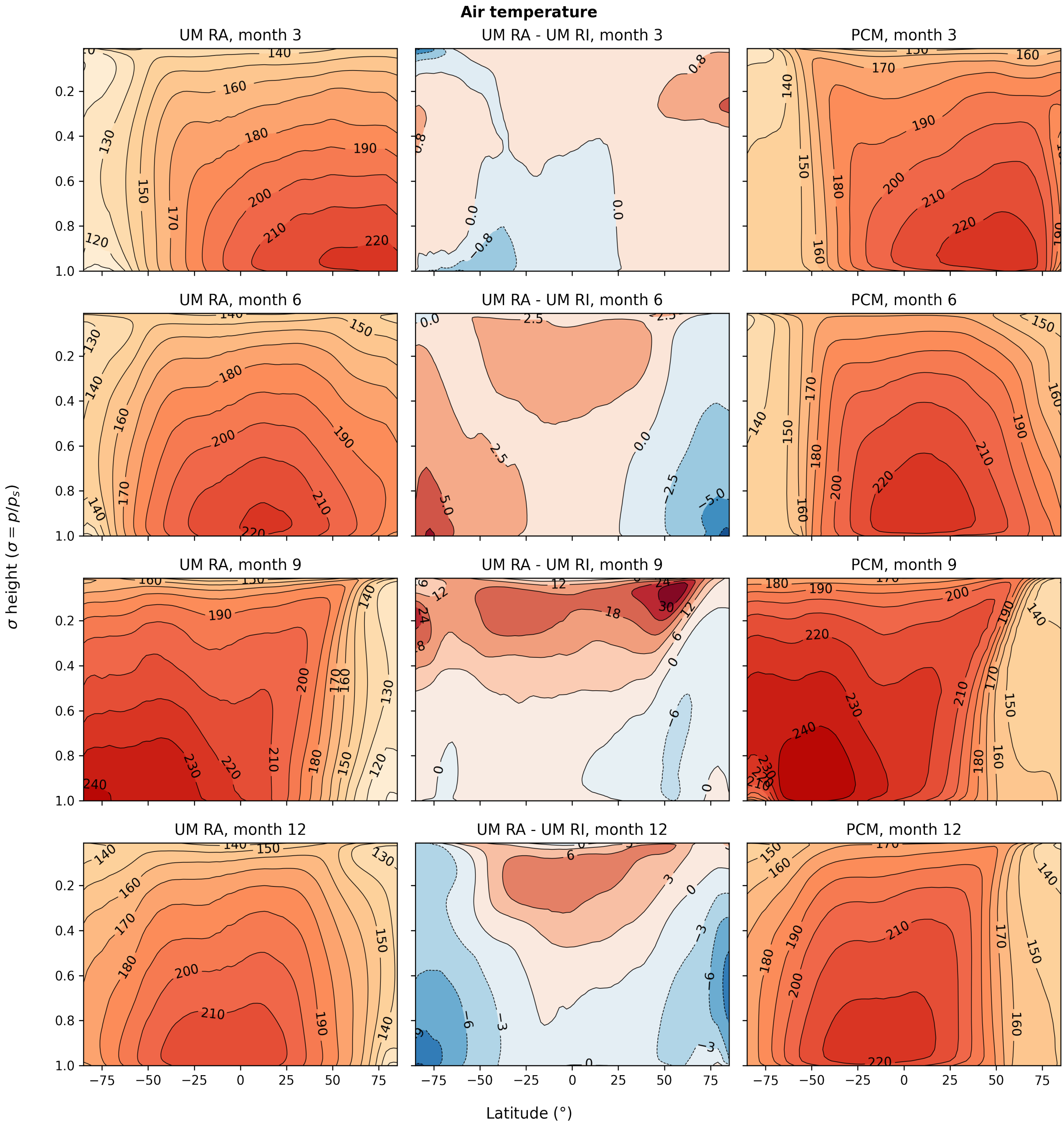

Figure 8. Zonal mean air temperature (K) across 4 seasons within the Martian year. For each month, the time average is taken of all sols within that month. The RA dust scenario is shown on the left, differences between the RA and RI dust scenario in the centre and PCM output on the right. Colour scales on the left-hand and right-hand plots are matched across all months and between models.

https://doi.org/10.5194/egusphere-2022-718
Preprint. Discussion started: 11 August 2022

4.2.3 Month 9

Month 9 is the peak of the dust season, and this is where differences between the RA and RI scenarios are greatest, as higher abundances of dust affect radiation fluxes more severely. Firstly, for both UM scenarios, dust (Fig. 9, month 9) is mainly concentrated in the SH forming a large 'plume' that extends vertically. Dust abundances have increased from earlier months and are now two orders of magnitude more than in month 3. The dust in the RA simulation is more concentrated at ∼30° S latitude, while RI dust is distributed more widely across latitudes, but with a minor difference towards ∼30° S latitude. This difference can clearly be seen with higher dust abundance at the equator at all altitudes for RA dust, compared to less dust nearer both poles than RI dust.

During colder months the temperatures are similar between UM scenarios, but during the dust season, the temperature differences are much more pronounced (Fig. 8, month 9). This change in magnitude of differences shows the effects of RA dust on temperature, highlighting how dust influences radiative transfer in Mars' atmosphere — particularly at mid-altitudes where dust can remain suspended influencing incoming solar radiation and outgoing thermal radiation from the surface. Temperatures (Fig. 8, month 9) near the surface are similar between scenarios, both being ∼20 K warmer than month 3, but at lower pressures (σ between ∼0.2 to 0.1) the RA dust scenario is considerably warmer (exceeding 30 K). This highlights the radiative effects of suspended atmospheric dust and how the climate might be different in its absence. Suspended atmospheric dust causes the upper atmosphere to be warmer than if there was no effects from dust (Fig. 9). In the scenario with RI dust, this dust layer does not affect radiation and solar radiation can reach the surface, however in the RA dust scenario, the suspended dust layer scatters incoming solar radiation transferring energy to the suspended dust layer instead of the surface. This 'band' of warmer air stretches from the mid-altitudes up to the top of atmosphere, across almost all latitudes (with an exception at the NH pole). Wind speed is a consequence of sharper temperature gradients due to the thermal wind balance relationship, so is affected by the disparity of temperature maximums between hemispheres. This can be seen by the higher wind speeds present in month 9 compared to month 3 (first columns in Fig. 6 and 7). Zonal winds (Fig. 6, month 9) feature more extreme differences between RA and RI simulations, ranging from -40 to 40 m s^{-1} in some places. These are mainly at the higher altitudes where temperature differences were at their greatest, above the dust layer. The polar jet in the RA dust scenario is considerably quicker but lacks an opposing jet near the top of the atmosphere in the SH (σ = 0.1, 50° S latitude), though this jet is small in the RI dust scenario (-20 m s^{-1}). RI dust does not feature an equatorial jet at the uppermost part of the simulated atmosphere (σ = <0.1). Meridional wind differences for this month (Fig. 7, month 9) are at their highest compared to other months, ranging from -3 to 3 m s^{-1} in the lower/middle atmosphere (σ = 1 to 0.5, 15° N latitude). A region near the top of atmosphere is faster in the RI dust scenario (up to 15 m s^{-1}, σ = 0.1, 15° N latitude).

Differences between the UM RA dust scenario and PCM during month 9 are at their least compared to other months (when compared at the relative ranges of the different months), suggesting the importance of radiatively active dust for reproducing the salient features of atmospheric dynamics on Mars. Dust MMR in both models is now much more comparable, with the UM having uplifted more dust than the PCM during prior months. Spatially, dust in the UM is concentrated in a large central plume at ∼30° S latitude, with dust in the PCM being more spread out across the atmosphere. The reasons for this are uncertain,

https://doi.org/10.5194/egusphere-2022-718
Preprint. Discussion started: 11 August 2022

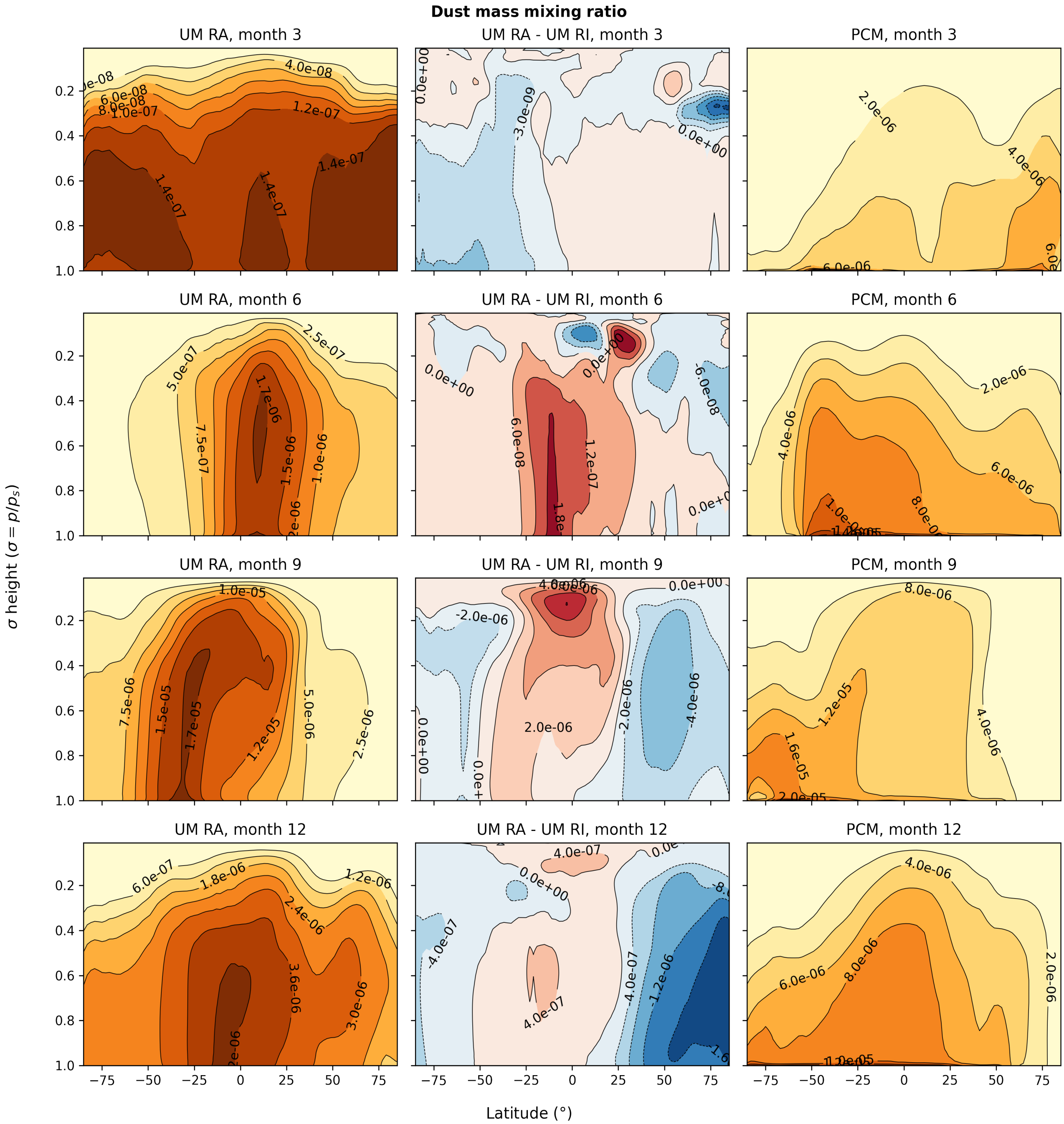

Figure 9. Zonal mean dust mass mixing ratio (kg kg^{-1}) across 4 seasons within the Martian year, each month is the average taken of all sols within that month (months according to Table A1). The RA dust scenario is shown on the left, differences between the RA and RI dust scenario in the centre and PCM output on the right. Contour lines denote mass mixing ratio and units are in kg kg^{-1}. Note that due to the wide range of values present between months, the colour scale ranges differ between months and models for this figure.

https://doi.org/10.5194/egusphere-2022-718
Preprint. Discussion started: 11 August 2022

but could potentially be the parameterisation of dust uplifting: the UM dynamically calculates dust reservoirs and horizontal flux, whereas PCM uses 'forced' dust injection to more closely match observations (Spiga et al., 2013; Montabone et al., 2015, 2020). This high vertical uplifting in the UM is responsible for a high input of dust into the atmosphere past the near-surface, a process described in detail by Spiga et al. (2013). Temperature differences between models exist throughout the atmosphere, with the largest differences occurring close to the surface at the poles and reaching -40 K in the NH pole and 40 K in the SH pole. These large differences are due to the current absence of ice at the poles in the UM, which will impact temperatures through emissivity and latent heat effects. The rest of the atmosphere is colder in the UM, with differences exceeding 20 K above the SH pole and above the equator at the upper edge of the simulated atmosphere. There is an agreement between models at the surface across the equator as in months 3 and 6, with another small area of agreement between models above the surface at σ = 0.9 to 0.2 and 50° N latitude. Zonal mean differences here are concentrated in the NH polar jet, with the rest of the atmosphere in agreement. The zonal NH polar jet in the UM is more spread out meridionally than the PCM, so the difference of 40 m s^{-1} at σ = 0.2, ∼60° N latitude is a result of the jet expanding horizontally in the UM rather than vertically as in the PCM. This is further highlighted by the -20 m s^{-1} difference at σ = 0.3, ∼45° N latitude, where the wind speeds in the UM are slower as a result of being more dispersed horizontally. Lastly, meridional wind differences between the UM and PCM in month 9 are not concentrated in a single jet or in a single direction, but instead occur sporadically throughout the atmosphere. There are some differences of -3 m s^{-1} near the surface and below the top of the simulated atmosphere, with 3 m s^{-1} faster wind speeds around the middle atmosphere (σ = 0.4, 0° and 20° S latitude) and top of the simulated atmosphere (σ = <0.1, 0° to 40° N latitude).

When discussing dust, month 9 is the most relevant of the four selected months, as it features the height of the dust season when dust is at its most abundant in both models. Our results show that we are able to simulate a dust cycle with intra-annual fluctuations in the UM without dust forcing. This month highlights the key takeaway from this study, that we have intra-annual dust quantity oscillation that is entirely reproduced dynamically by the GCM, with dust quantities rising during earlier months, peaking during the dust storm season and subsiding in later months.

4.2.4 Month 12

In month 12, the dust season ends and the atmosphere of Mars cools, the winds are weaker and dust MMR subsides while the polar jets transition between hemispheres. The uplifted dust quantities are considerably less than those of peak dust season, with RA scenarios still centred around the equator and RI dust shifting northward. Dust at the equator is more abundant in the RA scenario by $\sim 4.0 \times 10^{-7}$ kg kg^{-1} (∼10 % more dust in the RA scenario). Dust abundance is higher at the poles (mainly at the NH pole) in the RI dust scenario by -1.6×10^{-6} (∼40 % less dust in the RA scenario).

Overall, there is more dust uplifted in the RI scenario compared to the RA scenario, though this varies spatially (Fig. 9, month 12). Dust content in the RA scenario at the NH pole is less than that in the RI scenario by up to 1.6×10^{-6} kg kg^{-1} (∼187 %), with a similar but less extreme difference at the SH pole. Temperatures are beginning to decrease in this season and the warmest region is again in the lower latitudes in both scenarios (Fig. 8, month 12). The RI case is warmer at the equator in the upper atmosphere and colder near the poles in the lower atmosphere than that in the RA dust case. Zonal wind patterns

https://doi.org/10.5194/egusphere-2022-718
Preprint. Discussion started: 11 August 2022

change between hemispheres with higher polar jet speeds in both hemispheres for RA dust (Fig. 6, month 12). Differences in month 6 and 12 do switch hemispheres, but the magnitude of these differences is larger for month 12. This is likely caused by more residual dust in the atmosphere from month 9, causing temperature differences to be higher in month 12 than in month 6, in turn affecting the thermal wind relationship. This hemispheric reversal in the zonal wind mirrors what occurs in month 6, but is stronger in month 12 and stronger in the RA dust scenario, with maximum differences reaching now ∼20 m s^{-1} (compared to ∼10 m s^{-1} in month 6). Meridional winds for both scenarios show the Hadley cell direction reversal with the seasonal cycle (detailed by Read et al., 2015), wind speeds in both scenarios are once again comparable with the largest differences being between -3 to 1 m s^{-1}.

Comparison between the UM RA dust scenario and PCM shows similar trends as for month 6 in each variable, but inverted with respect to latitude (i.e. warmer temperature plume occurs in the NH instead of the SH, as in month 6). Temperatures are once again colder in the UM, but are generally colder than the differences in month 6 (i.e. month 6 differences ranged from -24/24 K, but month 12 ranges from -30/18 K). The UM again features a patch of warmer air at ∼60° N latitude up to ∼0.3 σ, but in the opposite hemisphere to month 6. There is also a small patch of colder air at the NH pole. These temperature discrepancies are likely to be the result of no polar ice in the UM which is present in the PCM (emissivity and thermal effects of polar ice are shown by Forget et al., 1998; Way et al., 2017). Throughout the rest of the atmosphere, as in month 6, the UM features lower air temperatures than those in the PCM, becoming lower as the height increases up to the top of atmosphere (Fig. 8, month 12). Zonal wind differences between models are quite varied during month 12, with varied wind speed differences across the upper atmosphere in both hemispheres and a weaker and wider polar jet in the NH (Fig. 6, month 12). The winds near the surface are quite comparable between models, but at the NH pole the wind speeds are faster in the UM, with this difference increasing with altitude up to ∼0.2 σ where the difference is ∼30 m s^{-1}. The entire NH polar jet in the UM is larger than the PCM, with the centre of the jet being spread out across more of the upper atmosphere, this is in contrast to the PCM where the NH polar jet is smaller but faster above ∼50° N latitude. The SH polar jet is also weaker in the UM, but this difference is much less than that of the NH (up to -10 K). Meridional winds differences are also similar to month 6 in locations, but differences where they do occur are less than in month 3. Once again there is a difference at ∼15° N latitude at ∼0.9 σ, but instead of -2 m s^{-1} as in month 6, its now 0 m s^{-1}.

Dust MMR fluctuates in both models throughout the year, becoming more abundant during month 9 (peak dust storm season, Fig. 9) then dissipating during the colder perihelion (9, month 3). Both outputs feature strong columns in the mid-latitudes spanning up into the mid-altitudes during dust season, with dust MMR being on average 2 orders of magnitude higher compared to that during colder months. Although there is an increase in dust MMR between seasons in both model outputs, the intensity of the change varies regionally, with poleward regions increasing less severely than equatorial regions.

Despite similarities between the RA and RI scenarios there are still some differences. Dust MMR is concentrated around the mid-latitudes for RA dust and is more dispersed with RI dust. Dust abundances are higher northward of the equator in the RI dust scenario during peak dust season (Fig. 9, month 9), but as the dust season subsides (approaching NH spring equinox) there are higher abundances of dust MMR in the RI scenarios towards the poles (Fig. 9, month 12). Because of this, months 6 and 12 are essential for monitoring dust uplifting rates.

https://doi.org/10.5194/egusphere-2022-718
Preprint. Discussion started: 11 August 2022

4.3 Variable comparison to the PCM

In this section we summarise the key differences between variables in the UMs RA simulation and the PCM output across the Martian year. We discuss zonal and meridional winds (Sect. 4.3.1), air temperature (Sect. 4.3.2) and dust (Sect. 4.3.3). We finish the section discussing the implications of dust differences between models and speculate as to their cause.

4.3.1 Winds

As shown in Fig. 6, overall patterns are similar between models, with both RA UM and PCM simulating strong eastward jets that alternate between hemispheres throughout the Martian seasons. Wind speed maxima in the PCM are generally faster than the UM, as is clearly seen in the plot for month 6 where the jets are present in both hemispheres, but are $\sim$30 m s^{-1} slower in the UM. This is likely due to less atmospheric dust around 0.6 σ in the UM which in turn leads to lower temperatures, this reduces pressure gradients causing slower winds (Madeleine et al., 2011). Despite these discrepancies, our results are encouraging, as they demonstrate the ability to model the major seasonal wind patterns with the UM.

As shown in Fig. 7, meridional wind patterns are similar between models, but do feature some key differences. In month 3, the jet at the upper boundary of the model is situated lower in the UM, relative to the PCM output, in addition to stronger surface winds in the UM. Month 6 features the largest differences, with more distinctive jets in the UM, that are more fragmented and overall weaker in the PCM output. Month 9 and 12 is highly similar between outputs, with the largest difference being a slightly faster mid-latitude jet in the UM during month 12.

4.3.2 Temperatures

As shown in Fig. 8, the differences in temperature between the UM and PCM outputs are notable throughout the year, the highest occurring in months 6 and 12. There is a consistent difference at the poles, this is likely due to the UM not having any form of polar ice and its effect on albedo and heat transfer (Forget et al., 1998, 1999). These missing parameterisations will have major impacts around the near-surface, as shown in Fig. 8 at the poles, with the effect weakening with height. Months 6 and 12 differences both feature patches where the UM simulations are warmer, at $\sim$60° in the hemisphere exiting winter ($\sim$-60° during month 3, $\sim$60° during month 12). Interestingly, the differences in temperature are small in months 3 and 9, despite the absence and presence of higher dust abundance, respectively. This occurs despite the difference in dust MMR maximum and minimum with month 3 being half the amount as month 9 (6×10^{-6} and 1.2×10^{-5}, respectively). This is likely due to the effects of dust uplifting and deposition (highest rate of change during months 6 and 12) having higher horizontal flux rates in the UM, leading to a non-uniform differences across the atmosphere. This is also suggested by the fairly consistent distribution of differences in temperatures during month 3 and 9, where the dust is at its least/most dust MMR, respectively, but dust uplifting and deposition rates are fairly homogeneous.

Across all months the PCM output is generally warmer than the UM, with the higher temperature differences correlating with months of higher dust differences (Fig. 8, month 9). This highlights the importance of atmospheric dust in thermal insulation in the Martian atmosphere, as temperatures nearer the upper boundary are cooler in the UM. This is likely caused by the lower

https://doi.org/10.5194/egusphere-2022-718
Preprint. Discussion started: 11 August 2022

amounts of suspended dust, compared to the PCM, allowing more solar radiation to the surface, causing a cooling gradient as height increases above the missing dust layer (Madeleine et al., 2011).

4.3.3 Dust content

Differences in dust distributions between the UM and PCM results are the most significant of all the variables, both throughout the year and regionally within monthly outputs. Differences between the dust amount vary greatly between models, with dust season total quantities being comparable but spatially varied, and the cold season retaining vastly more atmospheric dust in the PCM output than that in the RA UM scenario (Fig. 9). Whilst the PCM output during month 3 still has less uplifted dust than its dust season quantities, there is still significantly more dust in this month than the UM by ∼1.5 orders of magnitude. This disparity changes as both models approach the dust season (Fig. 9, month 6), however, with the dust uplifting rate in the UM being higher than the PCM. This means that there are initially large differences between the two models, but the UM is beginning to rectify the disparity between atmospheric dust amounts as it approaches the dust season. This becomes apparent in month 9 (Fig. 9, month 9) where the dust season is at its peak, both scenarios have much more similar amounts of dust in their outputs compared to previous months. Both outputs differ in their spatial distribution, with the UM featuring a large equatorial plume that extends into the upper atmosphere whilst the PCM features higher abundances at the SH pole. As the simulations progress towards month 12 (Fig. 9, month 12), dust abundances in the UM reduce faster than the PCM, resulting in higher dust abundance in the PCM output. This is a reversal of the observed pattern as seen in month 6, where UM dust uplifting was greater than the PCM, but instead the UM dust deposition is now stronger than the PCM output. This presents an interesting dilemma in understanding how these variables are represented in simulations, as the models do not have the same parameterizations for dust uplifting, and as a result there is a clear disparity in the amount of dust that can be uplifted between models. The usage of a 'free' dust scheme has also been explored by Neary and Daerden (2018) with the Global Environmental Multiscale model (further described by Husain et al., 2019). They are able to characterise the Martian atmosphere according to Mars year 27 using a 'free' dust scheme. Their work alongside this study emphasises the potential of a 'free' dust scheme, and also acts as a demonstration of model capabilities which we aim to explore further.

Although the cause for the disparity in dust distributions between those predicted by the UM and PCM is uncertain, we can speculate on potential causes. These might be caused by dust over-sensitivity to temperature in the UM. As the average atmospheric temperature decreases after the cold season, lower temperatures could potentially indirectly affect dust uplifting or deposition rates via slower wind speeds more severely in the UM, causing uplifted dust to decrease faster than anticipated. There are also consistent colder air temperatures in the UM, that vary in intensity throughout the Martian months, which could be amplifying this effect. Another reason might be that both models assume an infinite availability of dust reservoirs, which start uniformly distributed across the surface, but is allowed to develop and congregate in areas as the model progresses. This is currently an issue in Mars modelling, as the dust deposition in 'free' GCMs does not always match observations (Montabone et al., 2020). To rectify this, the PCM uses dust uplifting maps to dictate where dust is being forced into the atmosphere, as described by Madeleine et al. (2011); Spiga et al. (2013); Montabone et al. (2020). In our setup, the UM does not prescribe dust uplifting in such a way, but instead relies on the surface scheme to calculate dust reservoirs. Therefore, direct comparison

https://doi.org/10.5194/egusphere-2022-718
Preprint. Discussion started: 11 August 2022

to PCM output cannot be solely attributed to the difference in model parameterisation. Despite this, comparison of averaged seasonal trends does show both GCMs are able to capture annual dust storm seasons and non-dust seasons. Where dust is deposited in the model dictates source reservoirs for its subsequent uplifting. Therefore, understanding the deposition of dust and the formation of dust reservoirs (particularly after dust storms, due to the amount of dust transported) is therefore paramount to be able to reproduce the Martian dust cycle accurately (Montabone et al., 2015; Montabone and Forget, 2017; Forget and Montabone, 2017; Montabone et al., 2020). If certain regions are key contributors to dust uplifting, then misrepresenting the surface wind conditions over them would have a particularly noticeable effect for the global rate of dust uplifting. A third cause for such differences could be due to dust nucleation scavenging from CO_2 and H_2O condensation being present in the PCM, but absent in the UM. This affects global dust abundances where dust is being extracted from the atmosphere in the PCM during colder conditions. In the present paper, we focus only on dry simulations of the UM, so the dust abundance is not affected by scavenging from condensation, leading to potential over-estimation of dust abundance during the colder cloud season.

Rapid vertical dust uplifting ‘rocket dust storms’, as described by Spiga et al. (2013), play a key role in dust injection into the atmosphere. The PCM currently factors for this, but the UM dust scheme has not previously been required to simulate such intense vertical uplifting (since it does not feature on the same scale on Earth), therefore additional changes to the dust scheme are required in the UM. Observations and model comparison investigating this uplifting rate are essential to fine-tune the UM and verify if the UM captures this correctly, alongside determining whata developments or adjustments might be required to the UM dust scheme (Madeleine et al., 2011).

Both schemes omit some dust microphysics, namely surface crusting and surface re-entrainment (Woodward, 2001; Madeleine et al., 2011; Woodward et al., 2022), which likely contributes to the disparity between GCM outputs (without forcing) and observations. The differences in spatial distribution could also be caused by the differences in microphysics parameterisation between models, therefore refining this would undoubtedly improve representation of dust on Mars. The magnitude of this potential improvement, however, will remain uncertain until an inter-GCM comparison takes place where the initial and boundary conditions are identical. Such work would be able to identify differences which are solely due to these differences in parameterisations. Studies have been conducted on a mesoscale level in conjunction with the Mars 2020 lander (Newman et al., 2022), but took place prior to recent major improvements in parameterisations in current Mars GCMs (Kass et al., 2003; Madeleine et al., 2011; Spiga et al., 2013; Colaïtis et al., 2013; Navarro et al., 2014; González-Galindo et al., 2015). Global comparisons have been extensively applied to Earth GCMs through CMIP6 projects [4](Eyring et al., 2016). It has also been recently been conducted for exoplanets as part of the THAI project (described by Turbet et al., 2021; Sergeev et al., 2021; Fauchez et al., 2021), and the results have already identified new avenues for model improvement. . If such a comparison was applied to Mars GCMs, it would allow for identification of limitations of Mars modelling, potentially identifying limitations in our parameterisations, in turn allowing us to then improve comparisons to observations.

[4]Full list of projects available at https://www.wcrp-climate.org/modelling-wgcm-mip-catalogue/modelling-wgcm-cmip6-endorsed-mips

https://doi.org/10.5194/egusphere-2022-718
Preprint. Discussion started: 11 August 2022

5 Discussion and Conclusions

By using multiple GCMs to simulate Mars' climate in different ways, we are able to understand areas of inaccuracy within these models (González-Galindo et al., 2010; Hinson et al., 2014; Newman et al., 2021), as has been the case for Earth (e.g. Eyring et al., 2016), other Solar System bodies (e.g. Lora et al., 2019) and exoplanets (Turbet et al., 2021; Sergeev et al., 2021; Fauchez et al., 2021). With the UM we are able to simulate the same Martian climate in a different way compared to other models. These differences are present down to the core structure of the GCMs, with the UM being a non-hydrostatic model, different parameterisation for dust calculations and a height-based vertical structure. Using a non-hydrostatic model is especially relevant to Mars, as it features periodic pressure fluctuations which affect the entire climate in multiple ways (e.g. varying wind speeds and dust uplifting rates due less atmospheric mass, a summary of key differences between models is further highlighted by Turbet et al., 2021). Modelling comparable climates in different GCMs is crucial for identifying differences between them, potentially like those caused by parameterisation or as a result of the different methods used to calculate variables. This work and the developments with other Mars GCMs will undoubtedly allow us to eventually expand our capabilities in areas that currently elude us, such as being able to forecast when global dust storms will occur.

The UM is capable of reproducing salient features of the large-scale circulation, as we show in this paper, but lacks two key physical processes which have considerable impact on Mars' climate: water and CO_2 cycle. Including parameterizations for these processes is expected to further reduce the disparities between the UM and PCM. Our goal, however, is not to make our model identical to the PCM, but offer a new modelling framework that can complement the PCM (and other GCMs), while aiming for improvements in the aspects of Mars climate where current models struggle.

Firstly, by adding water vapour and radiatively active clouds, which would affect temperatures in a variety of ways (Navarro et al., 2014; Steele et al., 2017; Pál et al., 2019), in addition to dust uplifting rates (due to water acting as condensation nuclei for dust particles). The inclusion of these parameterizations would undoubtedly alter how the UM simulates Mars' dust and subsequently the planet's surface, especially as dust deposition changes surface properties such as thermal inertia or albedo (Bonev et al., 2008; Schmidt et al., 2009; Kahre and Haberle, 2010; Forget and Montabone, 2017). Although H_2O content is relatively low in the Martian atmosphere compared to other atmospheric compounds (even lower than Earth when accounting for the difference in atmospheric mass), it still is shown to have a large effect on Mars' climate. Radiatively active clouds can affect temperatures by up to 20 K (Madeleine et al., 2012; Navarro et al., 2014; Cooper et al., 2021) and moisture also affects dust nucleation and deposition (Walters et al., 2019). In the present study, we use the UM with a completely dry atmosphere similar to Turbet et al. (2021). However, as the UM has been originally developed for Earth, it already has two sophisticated cloud schemes which are routinely used for climate and weather prediction (described by Wilson et al., 2008b, a). Therefore, adding clouds to our setup would be a matter of adaptation of an existing scheme rather than a creation one from the ground up. Adding the hydrological cycle would affect dust deposition rates, especially during the colder months, when Mars relative humidity is at its highest. Temperature profiles would be different across the atmosphere (which will cause secondary effects on winds and dust MMR) as clouds influence radiation transfer. An example of this can be seen in Navarro et al. (2014) and the scenarios in the PCM.

https://doi.org/10.5194/egusphere-2022-718
Preprint. Discussion started: 11 August 2022

Secondly, our model needs to include a CO_2 cycle which substantially affects Mars' atmospheric pressure and the air-surface interaction at the poles in particular (as shown by Forget et al., 1999; Way et al., 2017). CO_2 condensation and sublimation leads to pressure fluctuations throughout the Martian year (Fig. 5), so it has to be accounted for by the model parameterizations to correctly reproduce horizontal pressure gradients, and thus the wind patterns (Haberle et al., 2008; Read et al., 2015; Martínez et al., 2017). In some GCMs, this has been tackled by fixing the available mass of atmospheric CO_2 to match the amount for the given pressure amount, which has allowed models to characterise an incredibly complicated process, enabling an idealised representation of Mars (Forget et al., 1999). More recently, work by Way et al. (2017) has been able to alter pressure levels throughout the simulation without such ad-hoc prescription. In a follow-up work, we are planning to implement this or a similar parameterization, and we expect this would improve year-round simulation as all prognostic variables shown in this paper would be affected by pressure variations, particularly during the colder months, where pressure difference between *Viking* lander observations and the UM are highest.

In this paper, we have shown the first application of the UM to a modern-day Mars climate, using a dry setup. We have demonstrated how we can adapt a highly sophisticated Earth climate model to simulate a climate on another planet. The UM demonstrates comparable wind patterns and temperature profiles to outputs from an established 3D Mars GCM, the PCM. We have shown how the UM is able to simulate seasonal temperature variations and its subsequent affects on winds. We have shown how the UM can simulate uplifted dust and identified areas of disparity during colder months where the absence of a CO_2 ice and hydrological scheme likely play a role. Future work will seek to use the existing moist physics in the UM as well as to implement a CO_2 condensation scheme, allowing for an interaction of these processes with dust — thus bringing more realism into our Mars simulations.

https://doi.org/10.5194/egusphere-2022-718
Preprint. Discussion started: 11 August 2022

Code availability. Scripts to process and visualise the post-processed UM data used in this study, alongside package requirements and tutorials, are available as a Zenodo dataset: https://doi.org/10.5281/zenodo.6974260 (McCulloch et al., 2022). If you do use those data then please cite this paper and add the following statement: "UM data have been obtained from https://doi.org/10.5281/zenodo.6974260".

Due to intellectual property right restrictions, we cannot provide either the source code or documentation papers for the UM or JULES. The Met Office Unified Model is available for use under licence. A number of research organisations and national meteorological services use the UM in collaboration with the Met Office to undertake basic atmospheric process research, produce forecasts, develop the UM code, and build and evaluate Earth system models. For further information on how to apply for a licence, see https://www.metoffice.gov.uk/research/approach/modelling-systems/unified-model (last access: 18 April 2022). Obtaining JULES. JULES is available under licence free of charge. For further information on how to gain permission to use JULES for research purposes, see http://jules-lsm.github.io/access_req/JULES_access.html (last access: 3 April 2022). UM–JULES simulations are compiled and run in suites developed using the Rose suite engine (http://metomi.github.io/rose/doc/html/index.html, MetOffice, 2020) and scheduled using the cylc workflow engine (urlhttps://cylc.github.io/, Oliver et al. (2019)). Both Rose and cylc are available under v3 of the GNU General Public License (GPL). In this framework, the suite contains the information required to extract and build the code as well as configure and run the simulations. Each suite is labelled with a unique identifier and is held in the same revision-controlled repository service in which we hold and develop the model code. This means that these suites are available to any licensed user of both the UM and JULES.

Appendix A: Appendix

In this section we include a reference table for matching Martian months and a reference table for vertical level height. In Table. A1, months can be matched with the respective solar longitude and amount of sols in that month. Mars features months that vary in their number of sols due to its orbital eccentricity, with less sols per month nearer perihelion and more sols per month closer to aphelion. Key months used in this study are months 3, 6, 9 and 12. In Table A2, vertical levels used in this configuration are given. Vertical levels are compressed/expanded depending on orography at any given point.

Author contributions. DMc led the writing and suite development with supervision from DS, NM, and MB. JM, BD and IB provided assistance in tuning the model and provided thorough descriptions on how they work. Paper reviewed and contributed to by all co-authors.

Competing interests. The authors declare that they have no conflict of interest.

Acknowledgements. We would like to thank the wider Exeter Exoplanet Theory Group for their feedback and support in UM development, as well as Patrick McGuire from the University of Reading for acting as a springboard for ideas. The authors also acknowledge the MCD data team: E. Millour, A. Spiga and F. Forget for providing freely accessible Mars climate data at http://www-mars.lmd.jussieu.fr/mars/info_web/index.html. Material produced using Met Office Software. We acknowledge use of the Monsoon2 system, a collaborative facility supplied under the Joint Weather and Climate Research Programme, a strategic partnership between the Met Office and the Natural Environment

https://doi.org/10.5194/egusphere-2022-718
Preprint. Discussion started: 11 August 2022

Table A1. Martian months, corresponding solar longitude (L_s) and amount of sols within that month. $0° L_s$ corresponds to Northern Hemisphere spring equinox.

Month	L_s	Sols
1	0 - 30	61
2	30 - 60	66
3	60 - 90	66
4	90 - 120	65
5	120 - 150	60
6	150 - 180	54
7	180 - 210	50
8	210 - 240	46
9	240 - 270	47
10	270 - 300	47
11	300 - 330	51
12	330 - 360	56

Research Council. This work was partly supported by a Science and Technology Facilities Council Consolidated Grant [ST/R000395/1], a Leverhulme Trust research project grant [RPG-2020-82] and a UKRI Future Leaders Fellowship [grant number MR/T040866/1]. For the purpose of open access, the authors have applied a Creative Commons Attribution (CC BY) licence to any Author Accepted Manuscript version arising.

Table A2. Vertical level heights used in our Mars setup. Values are given for a point at areoid height. This format allows for higher resolution at the surface.

θ levels – m height				
25.432	101.72	228.864	406.872	635.744
915.464	1246.056	1627.496	2059.8	2542.968
3076.992	3661.872	4297.616	4984.216	5721.672
6509.992	7349.176	8239.208	9180.112	10171.864
11214.48	12307.96	13452.288	14647.488	15893.536
17190.456	18538.224	19936.856	21386.344	22886.696
24387.088	25888.032	27391.424	28901.376	30425.168
31974.128	33564.536	35218.528	36964.968	38840.408
40889.92	43168.056	45739.696	48680.976	52080.208
56038.736	60671.856	66109.72	72498.248	80000
ρ levels – m height				
12.712	63.576	165.296	317.872	521.312
775.608	1080.76	1436.776	1843.648	2301.384
2809.976	3369.432	3979.744	4640.912	5352.944
6115.832	6929.584	7794.192	8709.656	9675.984
10693.176	11761.216	12880.128	14049.888	15270.512
16541.992	17864.336	19237.544	20661.6	22136.52
23636.888	25137.56	26639.728	28146.4	29663.272
31199.648	32769.336	34391.528	36091.744	37902.688
39865.168	42028.992	44453.872	47210.336	50380.592
54059.472	58355.296	63390.784	69303.984	76249.128

References

Aharonson, O., Zuber, M. T., Smith, D. E., Neumann, G. A., Feldman, W. C., and Prettyman, T. H.: Depth, distribution, and density of CO2 deposition on Mars, Journal of Geophysical Research E: Planets, 109, 1–10, https://doi.org/10.1029/2003JE002223, 2004.

Ball, E. R., Mitchell, D. M., Seviour, W. J. M., Thomson, S. I., and Vallis, G. K.: The Roles of Latent Heating and Dust in the Structure and Variability of the Northern Martian Polar Vortex, The Planetary Science Journal, 2, 203, https://doi.org/10.3847/psj/ac1ba2, 2021.

Banfield, D., Spiga, A., Newman, C., Forget, F., Lemmon, M., Lorenz, R., Murdoch, N., Viudez-Moreiras, D., Pla-Garcia, J., Garcia, R. F., Lognonné, P., Karatekin, , Perrin, C., Martire, L., Teanby, N., Hove, B. V., Maki, J. N., Kenda, B., Mueller, N. T., Rodriguez, S., Kawamura, T., McClean, J. B., Stott, A. E., Charalambous, C., Millour, E., Johnson, C. L., Mittelholz, A., Määttänen, A., Lewis, S. R., Clinton, J., Stähler, S. C., Ceylan, S., Giardini, D., Warren, T., Pike, W. T., Daubar, I., Golombek, M., Rolland, L., Widmer-Schnidrig, R., Mimoun, D., Beucler, E., Jacob, A., Lucas, A., Baker, M., Ansan, V., Hurst, K., Mora-Sotomayor, L., Navarro, S., Torres, J., Lepinette, A., Molina, A., Marin-Jimenez, M., Gomez-Elvira, J., Peinado, V., Rodriguez-Manfredi, J. A., Carcich, B. T., Sackett, S., Russell, C. T., Spohn, T., Smrekar, S. E., and Banerdt, W. B.: The atmosphere of Mars as observed by InSight, Nature Geoscience, 13, 190–198, https://doi.org/10.1038/s41561-020-0534-0, 2020.

Benacchio, T. and Wood, N.: Semi-implicit semi-Lagrangian modelling of the atmosphere: a Met Office perspective, Communications in Applied and Industrial Mathematics, 7, 4–25, https://doi.org/10.1515/caim-2016-0020, 2016.

Bonev, B. P., Hansen, G. B., Glenar, D. A., James, P. B., and Bjorkman, J. E.: Albedo models for the residual south polar cap on Mars: Implications for the stability of the cap under near-perihelion global dust storm conditions, Planetary and Space Science, 56, 181–193, https://doi.org/10.1016/j.pss.2007.08.003, 2008.

Boutle, I. A., Mayne, N. J., Drummond, B., Manners, J., Goyal, J., Hugo Lambert, F., Acreman, D. M., and Earnshaw, P. D.: Exploring the climate of Proxima B with the Met Office Unified Model, Astronomy and Astrophysics, 601, 1–13, https://doi.org/10.1051/0004-6361/201630020, 2017.

Boutle, I. A., Joshi, M., Lambert, F. H., Mayne, N. J., Lyster, D., Manners, J., Ridgway, R., and Kohary, K.: Mineral dust increases the habitability of terrestrial planets but confounds biomarker detection, Nature Communications, 11, 2731, https://doi.org/10.1038/s41467-020-16543-8, 2020.

Brown, A. J., Piqueux, S., and Titus, T. N.: Interannual observations and quantification of summertime H2O ice deposition on the Martian CO2 ice south polar cap, Earth and Planetary Science Letters, 406, 102–109, https://doi.org/10.1016/j.epsl.2014.08.039, 2014.

Chaffin, M. S., Kass, D. M., Aoki, S., Fedorova, A. A., Deighan, J., Connour, K., Heavens, N. G., Kleinböhl, A., Jain, S. K., Chaufray, J. Y., Mayyasi, M., Clarke, J. T., Stewart, A. I., Evans, J. S., Stevens, M. H., McClintock, W. E., Crismani, M. M., Holsclaw, G. M., Lefevre, F., Lo, D. Y., Montmessin, F., Schneider, N. M., Jakosky, B., Villanueva, G., Liuzzi, G., Daerden, F., Thomas, I. R., Lopez-Moreno, J. J., Patel, M. R., Bellucci, G., Ristic, B., Erwin, J. T., Vandaele, A. C., Trokhimovskiy, A., and Korablev, O. I.: Martian water loss to space enhanced by regional dust storms, Nature Astronomy, 5, 1036–1042, https://doi.org/10.1038/s41550-021-01425-w, 2021.

Colaïtis, A., Spiga, A., Hourdin, F., Rio, C., Forget, F., and Millour, E.: A thermal plume model for the Martian convective boundary layer, Journal of Geophysical Research: Planets, 118, 1468–1487, https://doi.org/10.1002/jgre.20104, 2013.

Cooper, B., Torre Juárez, M., Mischna, M., Lemmon, M., Martínez, G., Kass, D., Vasavada, A. R., Campbell, C., and Moores, J.: Thermal Forcing of the Nocturnal Near Surface Environment by Martian Water Ice Clouds, Journal of Geophysical Research: Planets, 126, 1–13, https://doi.org/10.1029/2020je006737, 2021.

Drummond, B., Mayne, N. J., Baraffe, I., Tremblin, P., Manners, J., Amundsen, D. S., Goyal, J., and Acreman, D.: The effect of metallicity on the atmospheres of exoplanets with fully coupled 3D hydrodynamics, equilibrium chemistry, and radiative transfer, Astronomy and Astrophysics, 612, 1–17, https://doi.org/10.1051/0004-6361/201732010, 2018.

Eager, J. K., Reichelt, D. J., Mayne, N. J., Hugo Lambert, F., Sergeev, D. E., Ridgway, R. J., Manners, J., Boutle, I. A., Lenton, T. M., and Kohary, K.: Implications of different stellar spectra for the climate of tidally locked Earth-like exoplanets, Astronomy and Astrophysics, 639, 1–12, https://doi.org/10.1051/0004-6361/202038089, 2020.

Edwards, J. M. and Slingo, A.: Studies with a flexible new radiation code. I: Choosing a configuration for a large-scale model, Quarterly Journal of the Royal Meteorological Society, 122, 689–719, https://doi.org/10.1256/smsqj.53106, 1996.

Eyring, V., Bony, S., Meehl, G. A., Senior, C. A., Stevens, B., Stouffer, R. J., and Taylor, K. E.: Overview of the Coupled Model Intercomparison Project Phase 6 (CMIP6) experimental design and organization, Geoscientific Model Development, 9, 1937–1958, https://doi.org/10.5194/gmd-9-1937-2016, 2016.

https://doi.org/10.5194/egusphere-2022-718
Preprint. Discussion started: 11 August 2022

Fauchez, T. J., Villanueva, G. L., Sergeev, D. E., Turbet, M., Boutle, I. A., Tsigaridis, K., Way, M. J., Wolf, E. T., Domagal-Goldman, S. D., Forget, F., Haqq-Misra, J., Kopparapu, R. K., Manners, J., and Mayne, N. J.: The TRAPPIST-1 Habitable Atmosphere Intercomparison (THAI). Part III: Simulated Observables – The return of the spectrum, Planetary Science Journal, http://arxiv.org/abs/2109.11460, 2021.

Fischer, E., Martínez, G. M., Rennó, N. O., Tamppari, L. K., and Zent, A. P.: Relative Humidity on Mars: New Results From the Phoenix TECP Sensor, Journal of Geophysical Research: Planets, 124, 2780–2792, https://doi.org/10.1029/2019JE006080, 2019.

Forget, F. and Montabone, L.: Atmospheric Dust on Mars: A Review, 47th International Conference on Environmental Systems, pp. 1–13, http://www-mars.lmd.jussieu.fr, 2017.

Forget, F., Hourdin, F., and Talagrand, O.: CO2 Snowfall on Mars: Simulation with a General Circulation Model, Icarus, 131, 302–316, https://doi.org/10.1006/icar.1997.5874, 1998.

Forget, F., Hourdin, F., Fournier, R., Hourdin, C., Talagrand, O., Collins, M., Lewis, S. R., Read, P. L., and Huot, J. P.: Improved general circulation models of the Martian atmosphere from the surface to above 80 km, Journal of Geophysical Research E: Planets, 104, 24 155–24 175, https://doi.org/10.1029/1999JE001025, 1999.

Gary-Bicas, C. E., Hayne, P. O., Horvath, T., Heavens, N. G., Kass, D. M., Kleinböhl, A., Piqueux, S., Shirley, J. H., Schofield, J. T., and McCleese, D. J.: Asymmetries in Snowfall, Emissivity, and Albedo of Mars' Seasonal Polar Caps: Mars Climate Sounder Observations, Journal of Geophysical Research: Planets, 125, https://doi.org/10.1029/2019JE006150, 2020.

Gebhardt, C., Abuelgasim, A., Fonseca, R. M., Martín-Torres, J., and Zorzano, M. P.: Fully Interactive and Refined Resolution Simulations of the Martian Dust Cycle by the MarsWRF Model, Journal of Geophysical Research: Planets, 125, 1–22, https://doi.org/10.1029/2019JE006253, 2020.

González-Galindo, F., Bougher, S. W., López-Valverde, M. A., Forget, F., and Murphy, J.: Thermal and wind structure of the Martian thermosphere as given by two General Circulation Models, Planetary and Space Science, 58, 1832–1849, https://doi.org/10.1016/j.pss.2010.08.013, 2010.

González-Galindo, F., López-Valverde, M. A., Forget, F., García-Comas, M., Millour, E., and Montabone, L.: Variability of the Martian thermosphere during eight Martian years as simulated by a ground-to-exosphere global circulation model, Journal of Geophysical Research: Planets, 120, 2020–2035, https://doi.org/10.1002/2015JE004925, 2015.

Haberle, R. M., McKay, C. P., Schaeffer, J., Cabrol, N. A., Grin, E. A., Zent, A. P., and Quinn, R.: On the possibility of liquid water on present-day Mars, Journal of Geophysical Research E: Planets, 106, 23 317–23 326, https://doi.org/10.1029/2000JE001360, 2001.

Haberle, R. M., Forget, F., Colaprete, A., Schaeffer, J., Boynton, W. V., Kelly, N. J., and Chamberlain, M. A.: The effect of ground ice on the Martian seasonal CO2 cycle, Planetary and Space Science, 56, 251–255, https://doi.org/10.1016/j.pss.2007.08.006, 2008.

Haberle, R. M., Kahre, M. A., Hollingsworth, J. L., Montmessin, F., Wilson, R. J., Urata, R. A., Brecht, A. S., Wolff, M. J., Kling, A. M., and Schaeffer, J. R.: Documentation of the NASA/Ames Legacy Mars Global Climate Model: Simulations of the present seasonal water cycle, Icarus, 333, 130–164, https://doi.org/10.1016/j.icarus.2019.03.026, 2019.

Hayne, P. O., Paige, D. A., Schofield, J. T., Kass, D. M., Kleinbhl, A., Heavens, N. G., and McCleese, D. J.: Carbon dioxide snow clouds on Mars: South polar winter observations by the Mars Climate Sounder, Journal of Geophysical Research E: Planets, 117, 1–23, https://doi.org/10.1029/2011JE004040, 2012.

Hébrard, E., Listowski, C., Coll, P., Marticorena, B., Bergametti, G., Määttänen, A., Montmessin, F., and Forget, F.: An aerodynamic roughness length map derived from extended Martian rock abundance data, Journal of Geophysical Research: Planets, 117, n/a–n/a, https://doi.org/10.1029/2011JE003942, 2012.

https://doi.org/10.5194/egusphere-2022-718
Preprint. Discussion started: 11 August 2022

Hinson, D. P., Asmar, S. W., Kahan, D. S., Akopian, V., Haberle, R. M., Spiga, A., Schofield, J. T., Kleinböhl, A., Abdou, W. A., Lewis, S. R., Paik, M., and Maalouf, S. G.: Initial results from radio occultation measurements with the Mars Reconnaissance Orbiter: A nocturnal mixed layer in the tropics and comparisons with polar profiles from the Mars Climate Sounder, Icarus, 243, 91–103, https://doi.org/10.1016/j.icarus.2014.09.019, 2014.

Holmes, J. A., Lewis, S. R., Patel, M. R., and Lefèvre, F.: A reanalysis of ozone on Mars from assimilation of SPICAM observations, Icarus, 302, 308–318, https://doi.org/10.1016/j.icarus.2017.11.026, 2018.

Houben, H., Haberle, R. M., Young, R. E., and Zent, A. P.: Evolution of the Martian water cycle, Advances in Space Research, 19, 1233–1236, https://doi.org/10.1016/S0273-1177(97)00274-3, 1997.

Husain, S. Z., Girard, C., Qaddouri, A., and Plante, A.: A new dynamical core of the Global Environmental Multiscale (GEM) model with a height-based terrain-following vertical coordinate, Monthly Weather Review, 147, 2555–2578, https://doi.org/10.1175/MWR-D-18-0438.1, 2019.

Jakosky, B. M. and Edwards, C. S.: Inventory of CO2 available for terraforming Mars, Nature Astronomy, 2, 634–639, https://doi.org/10.1038/s41550-018-0529-6, 2018.

Kahre, M. A. and Haberle, R. M.: Mars CO2 cycle: Effects of airborne dust and polar cap ice emissivity, Icarus, 207, 648–653, https://doi.org/10.1016/j.icarus.2009.12.016, 2010.

Kass, D. M., Schofield, J. T., Michaels, T. I., Rafkin, S. C., Richardson, M. I., and Toigo, A. D.: Analysis of atmospheric mesoscale models for entry, descent, and landing, Journal of Geophysical Research E: Planets, 108, 1–12, https://doi.org/10.1029/2003je002065, 2003.

Kass, D. M., Schofield, J. T., Kleinböhl, A., McCleese, D. J., Heavens, N. G., Shirley, J. H., and Steele, L. J.: Mars Climate Sounder Observation of Mars' 2018 Global Dust Storm, Geophysical Research Letters, 47, 1–9, https://doi.org/10.1029/2019GL083931, 2020.

Lefèvre, F., Bertaux, J.-L., Clancy, R. T., Encrenaz, T., Fast, K., Forget, F., Lebonnois, S., Montmessin, F., and Perrier, S.: Heterogeneous chemistry in the atmosphere of Mars, Nature, 454, 971–975, https://doi.org/10.1038/nature07116, 2008.

Lines, S., Manners, J., Mayne, N. J., Goyal, J., Carter, A. L., Boutle, I. A., Lee, G. K., Helling, C., Drummond, B., Acreman, D. M., and Sing, D. K.: Exonephology: Transmission spectra from a 3D simulated cloudy atmosphere of HD 209458b, Monthly Notices of the Royal Astronomical Society, 481, 194–205, https://doi.org/10.1093/mnras/sty2275, 2018.

Lock, A. P., Brown, A. R., Bush, M. R., Martin, G. M., and Smith, R. N. B.: A New Boundary Layer Mixing Scheme. Part I: Scheme Description and Single-Column Model Tests, Monthly Weather Review, 128, 3187–3199, https://doi.org/10.1175/1520-0493(2000)128<3187:ANBLMS>2.0.CO;2, 2000.

Lora, J. M., Tokano, T., Vatant d'Ollone, J., Lebonnois, S., and Lorenz, R. D.: A model intercomparison of Titan's climate and low-latitude environment, Icarus, 333, 113–126, https://doi.org/10.1016/j.icarus.2019.05.031, 2019.

Lott, F. and Miller, M. J.: A new subgrid-scale orographic drag parametrization: Its formulation and testing, Quarterly Journal of the Royal Meteorological Society, 123, 101–127, https://doi.org/10.1002/qj.49712353704, 1997.

Madeleine, J. B., Forget, F., Millour, E., Montabone, L., and Wolff, M. J.: Revisiting the radiative impact of dust on Mars using the LMD Global Climate Model, Journal of Geophysical Research E: Planets, 116, 11 010, https://doi.org/10.1029/2011JE003855, 2011.

Madeleine, J.-B., Forget, F., Millour, E., Navarro, T., and Spiga, A.: The influence of radiatively active water ice clouds on the Martian climate, Geophysical Research Letters, 39, n/a–n/a, https://doi.org/10.1029/2012GL053564, 2012.

Malin, M. C., Caplinger, M. A., and Davis, S. D.: Observational evidence for an active surface reservoir of solid carbon dioxide on Mars, Science, 294, 2146–2148, https://doi.org/10.1126/science.1066416, 2001.

Manners, J., Vosper, S. B., and Roberts, N.: Radiative transfer over resolved topographic features for high-resolution weather prediction, Quarterly Journal of the Royal Meteorological Society, 138, 720–733, https://doi.org/10.1002/qj.956, 2012.

Martínez, G. M., Newman, C. N., De Vicente-Retortillo, A., Fischer, E., Renno, N. O., Richardson, M. I., Fairén, A. G., Genzer, M., Guzewich, S. D., Haberle, R. M., Harri, A. M., Kemppinen, O., Lemmon, M. T., Smith, M. D., de la Torre-Juárez, M., and Vasavada, A. R.: The Modern Near-Surface Martian Climate: A Review of In-situ Meteorological Data from Viking to Curiosity, Space Science Reviews, 212, 295–338, https://doi.org/10.1007/s11214-017-0360-x, 2017.

Mayne, N. J., Baraffe, I., Acreman, D. M., Smith, C., Wood, N., Amundsen, D. S., Thuburn, J., and Jackson, D. R.: Using the UM dynamical cores to reproduce idealised 3-D flows, Geoscientific Model Development, 7, 3059–3087, https://doi.org/10.5194/gmd-7-3059-2014, 2014.

Mayne, N. J., Drummond, B., Debras, F., Jaupart, E., Manners, J., Boutle, I. A., Baraffe, I., and Kohary, K.: The Limits of the Primitive Equations of Dynamics for Warm, Slowly Rotating Small Neptunes and Super Earths, The Astrophysical Journal, 871, 56, https://doi.org/10.3847/1538-4357/aaf6e9, 2019.

McCulloch, D., Sergeev, D., Mayne, N., Bate, M., Manners, J., Boutle, I., and Drummond, B.: UM post-processed Mars dataset, https://doi.org/10.5281/zenodo.6974260, 2022.

Millour, E., Forget, F., Spiga, A., López-Valverde, M. A., Vals, M., Zakharov, A. V., Montabone, L., Lefevre, F., Montmessin, F., Chaufray, J. Y., González-Galindo, F., Lewis, S. R., Read, P. L., Desjean, M.-C., and Cipriani, F.: THE MARS CLIMATE DATABASE (VERSION 5.3), in: Scientific Workshop: "From Mars Express to ExoMars", ESAC Madrid, Spain, https://www.cosmos.esa.int/documents/1499429/1583871/Millour_E.pdf, 2018.

Montabone, L. and Forget, F.: FORECASTING DUST STORMS ON MARS: A SHORT REVIEW., vol. 2017, pp. 2–4, 2017.

Montabone, L., Lewis, S. R., Read, P. L., and Withers, P.: Reconstructing the weather on Mars at the time of the MERs and Beagle 2 landings, Geophysical Research Letters, 33, 1–5, https://doi.org/10.1029/2006GL026565, 2006.

Montabone, L., Forget, F., Millour, E., Wilson, R. J., Lewis, S. R., Cantor, B., Kass, D., Kleinböhl, A., Lemmon, M. T., Smith, M. D., and Wolff, M. J.: Eight-year climatology of dust optical depth on Mars, Icarus, 251, 65–95, https://doi.org/10.1016/j.icarus.2014.12.034, 2015.

Montabone, L., Spiga, A., Kass, D. M., Kleinböhl, A., Forget, F., and Millour, E.: Martian Year 34 Column Dust Climatology from Mars Climate Sounder Observations: Reconstructed Maps and Model Simulations, Journal of Geophysical Research: Planets, 125, https://doi.org/10.1029/2019JE006111, 2020.

Mulholland, D. P., Read, P. L., and Lewis, S. R.: Simulating the interannual variability of major dust storms on Mars using variable lifting thresholds, Icarus, 223, 344–358, https://doi.org/10.1016/j.icarus.2012.12.003, 2013.

Navarro, T., Madeleine, J. B., Forget, F., Spiga, A., Millour, E., Montmessin, F., and Määttänen, A.: Global climate modeling of the Martian water cycle with improved microphysics and radiatively active water ice clouds, Journal of Geophysical Research: Planets, 119, 1479–1495, https://doi.org/10.1002/2013JE004550, 2014.

Nazari-Sharabian, M., Aghababaei, M., Karakouzian, M., and Karami, M.: Water on Mars-A literature review, vol. 8, https://doi.org/10.3390/GALAXIES8020040, 2020.

Neakrase, L. D., Balme, M. R., Esposito, F., Kelling, T., Klose, M., Kok, J. F., Marticorena, B., Merrison, J., Patel, M., and Wurm, G.: Particle Lifting Processes in Dust Devils, Space Science Reviews, 203, 347–376, https://doi.org/10.1007/s11214-016-0296-6, 2016.

Neary, L. and Daerden, F.: The GEM-Mars general circulation model for Mars: Description and evaluation, Icarus, 300, 458–476, https://doi.org/10.1016/j.icarus.2017.09.028, 2018.

Newman, C. E., de la Torre Juárez, M., Pla-García, J., Wilson, R. J., Lewis, S. R., Neary, L., Kahre, M. A., Forget, F., Spiga, A., Richardson, M. I., Daerden, F., Bertrand, T., Viúdez-Moreiras, D., Sullivan, R., Sánchez-Lavega, A., Chide, B., and Rodriguez-Manfredi, J. A.: Multi-model Meteorological and Aeolian Predictions for Mars 2020 and the Jezero Crater Region, Space Science Reviews, 217, https://doi.org/10.1007/s11214-020-00788-2, 2021.

Newman, C. E., Bertrand, T., Fenton, L. K., Guzewich, S. D., Jackson, B., Lewis, S. R., Mischna, M. A., Montabone, L., and Wellington, D. F.: Martian Dust, January, Elsevier Inc., 2 edn., https://doi.org/10.1016/b978-0-12-818234-5.00143-7, 2022.

Oliver, H., Shin, M., Matthews, D., Sanders, O., Bartholomew, S., Clark, A., Fitzpatrick, B., Van Haren, R., Drost, N., and Hut, R.: Workflow Automation for Cycling Systems, Computing in Science and Engineering, 21, 7–21, https://doi.org/10.1109/MCSE.2019.2906593, 2019.

Paige, D. A. and Wood, S. E.: Modeling the Martian seasonal CO2 cycle 2. Interannual variability, Icarus, 99, 15–27, https://doi.org/10.1016/0019-1035(92)90167-6, 1992.

Pál, B., Kereszturi, , Forget, F., and Smith, M. D.: Global seasonal variations of the near-surface relative humidity levels on present-day Mars, Icarus, 333, 481–495, https://doi.org/10.1016/j.icarus.2019.07.007, 2019.

Pollack, J. B., Haberle, R. M., Murphy, J. R., Schaeffer, J., and Lee, H.: Simulations of the general circulation of the Martian atmosphere. 2. Seasonal pressure variations, Journal of Geophysical Research, 98, 3149–3181, https://doi.org/10.1029/92JE02947, 1993.

Pottier, A., Forget, F., Montmessin, F., Navarro, T., Spiga, A., Millour, E., Szantai, A., and Madeleine, J.-B.: Unraveling the martian water cycle with high-resolution global climate simulations, Icarus, 291, 82–106, https://doi.org/10.1016/j.icarus.2017.02.016, 2017.

Read, P. L., Lewis, S. R., and Mulholland, D. P.: The physics of Martian weather and climate: a review, Reports on Progress in Physics, 78, 125 901, https://doi.org/10.1088/0034-4885/78/12/125901, 2015.

Richardson, M. I. and Wilson, R. J.: A topographically forced asymmetry in the martian circulation and climate, Nature, 416, 298–301, https://doi.org/10.1038/416298a, 2002.

Schmidt, F., Douté, S., Schmitt, B., Vincendon, M., Bibring, J. P., and Langevin, Y.: Albedo control of seasonal South Polar cap recession on Mars, Icarus, 200, 374–394, https://doi.org/10.1016/j.icarus.2008.12.014, 2009.

Sergeev, D. E., Lambert, F. H., Mayne, N. J., Boutle, I. A., Manners, J., and Kohary, K.: Atmospheric Convection Plays a Key Role in the Climate of Tidally Locked Terrestrial Exoplanets: Insights from High-resolution Simulations, The Astrophysical Journal, 894, 84, https://doi.org/10.3847/1538-4357/ab8882, 2020.

Sergeev, D. E., Fauchez, T. J., Turbet, M., Boutle, I. A., Tsigaridis, K., Way, M. J., Wolf, E. T., Domagal-Goldman, S. D., Forget, F., Haqq-Misra, J., Kopparapu, R. K., Lambert, F. H., Manners, J., and Mayne, N. J.: The TRAPPIST-1 Habitable Atmosphere Intercomparison (THAI). Part II: Moist Cases – The Two Waterworlds, Planetary Science Journal, http://arxiv.org/abs/2109.11459, 2021.

Shaposhnikov, D. S., Rodin, A. V., and Medvedev, A. S.: The water cycle in the general circulation model of the martian atmosphere, Solar System Research, 50, 90–101, https://doi.org/10.1134/S0038094616020039, 2016.

Shaposhnikov, D. S., Rodin, A. V., Medvedev, A. S., Fedorova, A. A., Kuroda, T., and Hartogh, P.: Modeling the Hydrological Cycle in the Atmosphere of Mars: Influence of a Bimodal Size Distribution of Aerosol Nucleation Particles, Journal of Geophysical Research: Planets, 123, 508–526, https://doi.org/10.1002/2017JE005384, 2018.

Singh, D., Flanner, M. G., and Millour, E.: Improvement of Mars Surface Snow Albedo Modeling in LMD Mars GCM With SNICAR, Journal of Geophysical Research: Planets, 123, 780–791, https://doi.org/10.1002/2017JE005368, 2018.

Smith, D. E., Zuber, M. T., Solomon, S. C., Phillips, R. J., Head, J. W., Garvin, J. B., Banerdt, W. B., Muhleman, D. O., Pettengill, G. H., Neumann, G. A., Lemoine, F. G., Abshire, J. B., Aharonson, O., Brown, C. D., Hauck, S. A., Ivanov, A. B., McGovern, P. J., Zwally, H. J., and Duxbury, T. C.: The global topography of Mars and implications for surface evolution, Science, 284, 1495–1503, https://doi.org/10.1126/science.284.5419.1495, 1999.

Spafford, L. and Macdougall, A. H.: Validation of terrestrial biogeochemistry in CMIP6 Earth system models: A review, Geoscientific Model Development, 14, 5863–5889, https://doi.org/10.5194/gmd-14-5863-2021, 2021.

Spiga, A. and Forget, F.: A new model to simulate the Martian mesoscale and microscale atmospheric circulation: Validation and first results, Journal of Geophysical Research E: Planets, 114, 1–26, https://doi.org/10.1029/2008JE003242, 2009.

Spiga, A., Faure, J., Madeleine, J. B., Määttänen, A., and Forget, F.: Rocket dust storms and detached dust layers in the Martian atmosphere, Journal of Geophysical Research E: Planets, 118, 746–767, https://doi.org/10.1002/jgre.20046, 2013.

Spiga, A., Hinson, D. P., Madeleine, J. B., Navarro, T., Millour, E., Forget, F., and Montmessin, F.: Snow precipitation on Mars driven by cloud-induced night-time convection, Nature Geoscience, 10, 652–657, https://doi.org/10.1038/ngeo3008, 2017.

Staniforth, A. and Wood, N.: The deep-atmosphere Euler equations in a generalized vertical coordinate, Monthly Weather Review, 131, 1931–1938, https://doi.org/10.1175//2564.1, 2003.

Staniforth, A. and Wood, N.: Aspects of the dynamical core of a nonhydrostatic, deep-atmosphere, unified weather and climate-prediction model, Journal of Computational Physics, 227, 3445–3464, https://doi.org/10.1016/j.jcp.2006.11.009, 2008.

Steele, L. J., Balme, M. R., Lewis, S. R., and Spiga, A.: The water cycle and regolith–atmosphere interaction at Gale crater, Mars, Icarus, 289, 56–79, https://doi.org/10.1016/j.icarus.2017.02.010, 2017.

Streeter, P. M., Lewis, S. R., Patel, M. R., Holmes, J. A., and Kass, D. M.: Surface Warming During the 2018/Mars Year 34 Global Dust Storm, Geophysical Research Letters, 47, 1–11, https://doi.org/10.1029/2019GL083936, 2020.

Tillman, J. E.: VL1/VL2-M-MET-4-DAILY-AVG-PRESSURE-V1.0, https://atmos.nmsu.edu/data_and_services/atmospheres_data/MARS/viking/sol_avg_sur_press_data.html, 1989.

Turbet, M., Fauchez, T. J., Sergeev, D. E., Boutle, I. A., Tsigaridis, K., Way, M. J., Wolf, E. T., Domagal-Goldman, S. D., Forget, F., Haqq-Misra, J., Kopparapu, R. K., Lambert, F. H., Manners, J., Mayne, N. J., and Sohl, L.: The TRAPPIST-1 Habitable Atmosphere Intercomparison (THAI). Part I: Dry Cases – The fellowship of the GCMs, Planetary Science Journal, pp. 1–23, http://arxiv.org/abs/2109.11457, 2021.

Vosper, S. B.: Mountain waves and wakes generated by South Georgia: Implications for drag parametrization, Quarterly Journal of the Royal Meteorological Society, 141, 2813–2827, https://doi.org/10.1002/qj.2566, 2015.

Walters, D., Baran, A. J., Boutle, I., Brooks, M., Earnshaw, P., Edwards, J., Furtado, K., Hill, P., Lock, A., Manners, J., Morcrette, C., Mulcahy, J., Sanchez, C., Smith, C., Stratton, R., Tennant, W., Tomassini, L., Van Weverberg, K., Vosper, S., Willett, M., Browse, J., Bushell, A., Carslaw, K., Dalvi, M., Essery, R., Gedney, N., Hardiman, S., Johnson, B., Johnson, C., Jones, A., Jones, C., Mann, G., Milton, S., Rumbold, H., Sellar, A., Ujiie, M., Whitall, M., Williams, K., and Zerroukat, M.: The Met Office Unified Model Global Atmosphere 7.0/7.1 and JULES Global Land 7.0 configurations, Geoscientific Model Development, 12, 1909–1963, https://doi.org/10.5194/gmd-12-1909-2019, 2019.

Wang, C., Forget, F., Bertrand, T., Spiga, A., Millour, E., and Navarro, T.: Parameterization of Rocket Dust Storms on Mars in the LMD Martian GCM: Modeling Details and Validation, Journal of Geophysical Research: Planets, 123, 982–1000, https://doi.org/10.1002/2017JE005255, 2018.

Wang, H. and Richardson, M. I.: The origin, evolution, and trajectory of large dust storms on Mars during Mars years 24-30 (1999-2011), Icarus, 251, 112–127, https://doi.org/10.1016/j.icarus.2013.10.033, 2015.

https://doi.org/10.5194/egusphere-2022-718
Preprint. Discussion started: 11 August 2022

Way, M. J., Aleinov, I., Amundsen, D. S., Chandler, M. A., Clune, T. L., Genio, A. D. D., Fujii, Y., Kelley, M., Kiang, N. Y., Sohl, L., and Tsigaridis, K.: Resolving Orbital and Climate Keys of Earth and Extraterrestrial Environments with Dynamics (ROCKE-3D) 1.0: A General Circulation Model for Simulating the Climates of Rocky Planets, The Astrophysical Journal Supplement Series, 231, 12, https://doi.org/10.3847/1538-4365/aa7a06, 2017.

Webster, S., Brown, A. R., Cameron, D. R., and Jones, C. P.: Improvements to the representation of orography in the Met Office Unified Model, Quarterly Journal of the Royal Meteorological Society, 129, 1989–2010, https://doi.org/10.1256/qj.02.133, 2003.

Wilson, D. R., Bushell, A. C., Kerr-Munslow, A. M., Price, J. D., and Morcrette, C. J.: PC2: A prognostic cloud fraction and condensation scheme. I: Scheme description, Quarterly Journal of the Royal Meteorological Society, 134, 2093–2107, https://doi.org/10.1002/qj.333, 2008a.

Wilson, D. R., Bushell, A. C., Kerr-Munslow, A. M., Price, J. D., Morcrette, C. J., and Bodas-Salcedo, A.: PC2: A prognostic cloud fraction and condensation scheme. II: Climate model simulations, Quarterly Journal of the Royal Meteorological Society, 134, 2109–2125, https://doi.org/10.1002/qj.332, 2008b.

Wood, N., Staniforth, A., White, A., Allen, T., Diamantakis, M., Gross, M., Melvin, T., Smith, C., Vosper, S., Zerroukat, M., and Thuburn, J.: An inherently mass-conserving semi-implicit semi-Lagrangian discretization of the deep-atmosphere global non-hydrostatic equations, Quarterly Journal of the Royal Meteorological Society, 140, 1505–1520, https://doi.org/10.1002/qj.2235, 2014.

Woodward, S.: Modeling the atmospheric life cycle and radiative impact of mineral dust in the Hadley Centre climate model, Journal of Geophysical Research: Atmospheres, 106, 18 155–18 166, https://doi.org/https://doi.org/10.1029/2000JD900795, 2001.

Woodward, S.: Mineral Dust in HadGEM 2 Technical Report 87, Tech. Rep. March, Met Office, Hadley Centre, Met Office, Exeter, https://sds-was.aemet.es/forecast-products/dust-forecasts/Woodward_2011_HadGEM2.pdf, 2011.

Woodward, S., Sellar, A., Tang, Y., Stringer, M., Yool, A., Robertson, E., and Wiltshire, A.: The simulation of mineral dust in the United Kingdom Earth System Model UKESM1, Atmospheric Chemistry and Physics, in review, https://doi.org/https://doi.org/10.5194/acp-2022-228, 2022.

Zalucha, A. M., Plumb, R. A., and Wilson, R. J.: An Analysis of the Effect of Topography on the Martian Hadley Cells, Journal of the Atmospheric Sciences, 67, 673–693, https://doi.org/10.1175/2009JAS3130.1, 2010.